Table 2　SREBP1c による影響およびカロリー制限における SREBP1c の影響

	SREBP1cKO による影響	CR による影響			
		野生型マウス		SREBP1cKO マウス	
		摂食後	摂食前	摂食後	摂食前
寿命	↓	↑		→	
呼吸商	↑	↓		↓	
グルコース負荷試験	→	↑		→	
インスリン負荷試験	→	↑		→	
腹部内臓脂肪組織量	↓	↓↓		↓	
肩甲骨間褐色脂肪組織量	→	↓		→	
血液生化学					
トリグリセリド	→	→	↓	→	→
遊離脂肪酸	→	↓	↓	→	→
ケトン体	↓	un	↓	un	→
肝臓含有脂質					
トリグリセリド	→	→	↓	→	↓
遊離脂肪酸	↑	→	→	→	→
心臓含有脂質					
トリグリセリド	→	→	→	→	→
遊離脂肪酸	→	→	↑	→	→

un：undetectable

いる[16)~18)]．すなわち，脂肪細胞の代謝や分化，アディポカインは寿命制御に重要であることが示唆される．

一方，CR による個体のサイズや体重の減少は，脂肪組織量の減少を伴う．CR は体重に比べ脂肪組織量，さらには内臓脂肪量により強い影響を与えるといわれている[19)]．われわれは，CR 群および対照群の精巣上体周囲白色脂肪組織での網羅的遺伝子発現解析を行い，CR が多くの糖，アミノ酸，脂質およびミトコンドリアエネルギー代謝関連遺伝子の発現を増強すること，一方，多くの炎症，血管新生，細胞外器質および細胞骨格関連遺伝子の発現を抑制することを明らかにした[20)21)]．このような遺伝子発現の変化は，摂食パターンに影響を受けなかった．また，遺伝子発現の変化の一部は，*in vitro* での脂肪細胞の分化に伴う遺伝子発現の変化と同様であり，一方，すでに報告されている肥満動物の脂肪組織での遺伝子発現とは，逆相関する傾向を示した[20)21)]．さらに，CR ラットおよび Tg ラット，AL ラットの精巣上体周囲脂肪組織において，形態学的および網羅的遺伝子発現解析を行った．その結果，AL ラットに比較して，CR ラットの脂肪細胞のサイズは顕著に小型化したが，Tg ラットでの変化は乏しかった．また，CR ラットでは脂肪酸合成関連遺伝子の発現が亢進し，炎症関連遺伝子の発現は抑制されたが，このような遺伝子発現の変化は Tg ラットでは観察されなかった（**Table 1**）．さらに，CR ラットでのみ発現が亢進した脂肪酸合成関連遺伝子の多くは脂肪酸合成系のマスター転写調節因子である sterol regulatory element binding protein (SREBP) 1 により制御される遺伝子群であった（未発表データ）．

以上より，血中の遊離脂肪酸およびケトン体レベルの変化，肝臓におけるミトコンドリア β 酸化と脂肪酸合成関連遺伝子発現の変化，脂肪組織における *de novo* 脂肪酸合成と炎症関連遺伝子の発現の変化，すなわち脂質代謝の変化と脂肪組織のリモデリングが，GH/IGF-1 シグナル非依存的な CR による変化と考えられ，その一部は SREBP1 により制御されている可能性が示唆された．

適応反応仮説からみたCRによる代謝の変化におけるSREBP1cの関与

さまざまなパラメーターにおいて，CRは絶食状態（fasting，starvation）とは異なるが，血中レプチン，インスリン，成長ホルモンおよびLHレベルはともに低値を示し，コルチコステロンレベルは高値を示すという変化は共通している[22)23)]．また絶食状態では，呼吸商（respiratory quotient）は低値を示し，エネルギー源が糖質から脂質へシフトし[24)25)]，白色脂肪組織由来の脂肪酸が，ミトコンドリアβ酸化の燃料として使われ，主に脳における燃料源であるケトン体が作られる[25)]．CRラットの呼吸商は，食餌摂取後では高値，摂取前では低値を示し，その日内変動は食餌摂取に依存し大きく変動する．一方，ALラットの呼吸商の日内変動は，CRラットに比べて小さい[26)]．そこで，われわれはSREBP1cノックアウト（KO）マウスと野生型マウスにおのおのCRを行い，寿命をはじめとするさまざまなパラメーターの解析を行った．その結果を**Table 2**に示す．SREBP1cKOマウス（以下，KOマウス）では，野生型マウスに比べて，平均および最大寿命とも有意に減少した．野生型マウスではCRに伴い平均および最大寿命とも延長したが，興味深いことにKOマウスではこのCRに伴う寿命延長効果がみられなかった．KOマウスでは野生型に比べて呼吸商は有意に高値を示し，日内変動も乏しかった．しかしながら，CR時の呼吸商は野生型，KOマウスとも有意な差はみられなかった．グルコース負荷試験およびインスリン負荷試験において，野生型ではCRによりグルコース耐性，インスリン感受性が亢進したが，KOマウスではこのようなCRの効果は失われていた．腹部内臓脂肪はKOマウスにおいて減少していた．CRにより野生型では腹部内臓脂肪量は顕著に減少したものの，KOマウスではその減少が乏しかった．また，肩甲骨間褐色脂肪組織量はCRにより野生型マウスでは顕著に減少するものの，KOマウスではこの減少がみられなかった．血液や肝臓および心臓含有トリグリセリドや遊離脂肪酸においても，野生型において観察されたCRの影響がKOマウスでは観察できないものがあった．摂食前の空腹時ケトン体レベルは野生型マウスに比べてKOマウスで減少した．野生型マウスではCRの空腹時ケトン体レベルは有意に増加したが，KOマウスではこのような変化は観察できなかった．以上の知見から，KOマウスではCRにより脂質をエネルギー源として有効に利用する能力が低下しているのではないかと考えられた（未発表データ）．

そこで，野生型およびKOマウスでの絶食に対する応答を比較した．するとKOマウスでは野生型に比べて，絶食に伴って観察される体重の減少，脂肪組織重量の減少，血糖値の低下および血清ケトン体の増加が抑制されていることが明らかとなった（未発表データ）．このことは，SREBP1cが絶食応答，さらにCRによる抗老化・寿命延長効果に重要な役割を担っていることを示唆する．

de novo 脂肪酸合成の重要性

われわれはCRおよび自由摂食ラットの白色脂肪組織においてプロテオーム解析を行った．その結果，CRによりATP-citrate lyase，NADP-dependent malic enzyme，pyruvate dehydrogenase E1 component subunit beta，pyruvate carboxylaseの発現が増加していた．さらに，citrate synthase活性が亢進していた．このことは，CRによりピルビン酸/リンゴ酸回路が活性化している可能性を示唆する（未発表データ）．また，前述したようにCRによりSREBP1cを介した脂肪酸合成が亢進していた．この2つのCR動物の白色脂肪組織の特徴を考え合わせると，白色脂肪組織はCR時エネルギー貯蔵装置としてではなく，グルコースをよりエネルギー効率の高い脂肪酸に変換する装置として機能している可

能性を示唆する．一方，がん悪液質の白色脂肪組織では，CRと同じように摂食量が減少した状態にもかかわらず，SREBP1cを介した脂肪酸合成は抑制されているようである[27]．この違いは，白色脂肪組織での *de novo* 脂肪酸合成が亢進されるか抑制されるかが，生理的なやせか病的なやせかの違いの1つになる可能性を示唆する．

おわりに

CRに関する研究は，主として老化生物学を専門とする研究者により研究されてきており，現在，この分野でのCRに関する研究は，“その作用メカニズムの解明”に加え，“ヒトにおけるCRの有効性”という2つの主要テーマに集約されている．そのうち前者に関して，白色脂肪組織リモデリングとSREBP1cを介した脂質代謝活性化の重要性を述べた．一方，同じく摂食量が減少した病態として，がん悪液質や神経性食欲不振症などの摂食障害があり，近年，モデル動物を用いた研究が広く行われるようになってきた．一般にがん悪液質における脂肪組織の萎縮はlipolysisの亢進によると考えられており，脂肪酸合成に関する知見は乏しい[27]．今まで異なった分野で研究されてきたCRモデルおよび摂食障害モデルから得られる知見を比較，検討することで，両分野に新たな切り口での研究の進展が期待される．

謝辞：第52回日本心身医学会総会のシンポジウムにおける講演の機会，さらにこの総説を執筆する機会を与えてくださった乾　明夫先生ならびに須藤信行先生に感謝いたします．

文献

1) Yu BP：Modulation of Aging Processes by Dietary Restriction. CRC Press, Boca Raton, 1994
2) Weindruch R, Walford RL：The Retardation of Aging and Disease by Dietary Restriction. Charles C Thomas, Springfield, 1988
3) Holliday R：Food reproduction and longevity：Is the extended lifespan of calorie-restricted animals an evolutionary adaptation? *Bioessays* **10**：125-127, 1989
4) Higami Y, Yamaza H, Shimokawa I：Laboratory findings of caloric restriction in rodents and primates. *Adv Clin Chem* **39**：211-237, 2005
5) Masoro EJ：Overview of caloric restriction and ageing. *Mech Ageing Dev* **126**：913-922, 2005
6) Sinclair DA：Toward a unified theory of caloric restriction and longevity regulation. *Mech Ageing Dev* **126**：987-1002, 2005
7) Colman RJ, Anderson RM, Johnson SC, et al：Caloric restriction delays disease onset and mortality in rhesus monkeys. *Science* **325**：201-204, 2009
8) Kemnitz JW：Calorie restriction and aging in nonhuman primates. *ILAR J* **52**：66-77, 2011
9) Roth GS, Lane MA, Ingram DK, et al：Biomarkers of caloric restriction may predict longevity in humans. *Science* **297**：811, 2002
10) Brown-Borg HM, Borg KE, Meliska CJ, et al：Dwarf mice and the ageing process. *Nature* **384**：33, 1996
11) Shimokawa I, Chiba T, Yamaza H, et al：Longevity genes：insights from calorie restriction and genetic longevity models. *Mol Cells* **26**：427-435, 2008
12) Shimokawa I, Higami Y, Utsuyama M, et al：Life span extension by reduction in growth hormone-insulin-like growth factor-1 axis in a transgenic rat model. *Am J Pathol* **160**：2259-2265, 2002
13) Shimokawa I, Higami Y, Tsuchiya T, et al：Life span extension by reduction of the growth hormone-insulin-like growth factor-1 axis：relation to caloric restriction. *FASEB J* **17**：1108-1109, 2003
14) Higami Y, Tsuchiya T, Chiba T, et al：Hepatic gene expression profile of lipid metabolism in rats：Impact of caloric restriction and growth hormone/insulin-like growth factor-1 suppression. *J Gerontol A Biol Sci Med Sci* **61**：1099-1110, 2006
15) Yamaza H, Komatsu T, Chiba T, et al：A transgenic dwarf rat model as a tool for the study of calorie restriction and aging. *Exp Gerontol* **39**：269-272, 2004
16) Blüher M, Kahn BB, Kahn CR：Extended longevity in mice lacking the insulin receptor in adipose tissue. *Science* **299**：572-574, 2003
17) Chiu CH, Lin WD, Huang SY, et al：Effect of a C/EBP gene replacement on mitochondrial biogenesis in fat cells. *Genes Dev* **18**：1970-1975, 2004
18) Otabe S, Yuan X, Fukutani T, et al：Overexpression of human adiponectin in transgenic mice results in suppression of fat accumulation and

prevention of premature death by high-calorie diet. *Am J Physiol Endocrinol Metab* **293**: E210-218, 2007
19) Barzilai N, Banerjee S, Hawkins M, et al: Caloric restriction reverses hepatic insulin resistance in aging rats by decreasing visceral fat. *J Clin Invest* **101**: 1353-1361, 1998
20) Higami Y, Pugh TD, Page GP, et al: Adipose tissue energy metabolism: altered gene expression profile of mice subjected to long-term caloric restriction. *FASEB J* **18**: 415-417, 2004
21) Higami Y, Barger JL, Page GP, et al: Energy restriction lowers the expression of genes linked to inflammation, the cytoskeleton, the extracellular matrix, and angiogenesis in mouse adipose tissue. *J Nutr* **136**: 343-352, 2006
22) Nelson JF: Neuroendocrine involvement in the retardation of aging by dietary restriction: A hypothesis. In: Yu BP (ed): Modulation of Aging Processes by Dietary Restriction. Boca CRC Press, Raton, Florida, pp37-55, 1994
23) Ahima RS, Prabakaran D, Mantzoros C, et al: Role of leptin in the neuroendocrine response to fasting. *Nature* **382**: 250-252, 1996
24) Overton JM, Williams TD, Chambers JB, et al: Central leptin infusion attenuates the cardiovascular and metabolic effects of fasting in rats. *Hypertension* **37**: 663-669, 2001
25) Salway JG: Metabolism at a Glance. Blackwell Science, Oxford, UK, 1999
26) McCarter RJ, Palmer J: Energy metabolism and aging: a lifelong study of Fischer 344 rats. *Am J Physiol* **263**: E448-452, 1992
27) Bing C, Trayhurn P: New insights into adipose tissue atrophy in cancer cachexia. *Proc Nutr Soc* **68**: 385-392, 2009

Abstract

Altered Energy Metabolism in Anti-aging and Pro-longevity Effects of Caloric Restriction

Yoshikazu Higami*

*Molecular Pathology & Metabolic Disease, Faculty of Pharmaceutical Sciences, Tokyo University of Science
(*Mailing Address*: Yoshikazu Higami, 2641 Yamazaki, Noda-shi, Chiba 278-8510, Japan)

Caloric restriction (CR) has been applied as a powerful tool in aging research. CR is accepted as a robust, reproducible and simple experimental manipulation known to extend both median and maximum lifespans, and to retard and suppress a broad spectrum of pathophysiological changes in a variety of mammals. In general, CR delays skeletal and sexual maturation, reduces body size with less adiposity, lowers body temperature, modulates hyperglycemia and insulinemia, alters lipid and energy metabolisms, protects against internal oxidative and environmental stresses, and activates mitochondrial biogenesis and sirtuins. Based on the adaptive response hypothesis against food shortage, I propose that CR promotes adipose tissue remodeling and modulates energy metabolism via sterol regulatory element binding protein (SREBP) 1c, a master transcriptional factor of fatty acid biosynthesis. Activation of *de novo* fatty acid biosynthesis regulated by SREBP1c might play an important role in the anti-aging and lifespan extension by caloric restriction.

Key words: caloric restriction, aging, lipid metabolism, adipose tissue remodeling, SREBP1c

Biochemical and Biophysical Research Communications 421 (2012) 15–19

Contents lists available at SciVerse ScienceDirect

Biochemical and Biophysical Research Communications

journal homepage: www.elsevier.com/locate/ybbrc

Reversible induction of PARP1 degradation by p53-inducible cis-imidazoline compounds

Wataru Nagai [1], Naoyuki Okita *,[1], Hiroshi Matsumoto, Hitoshi Okado, Misako Oku, Yoshikazu Higami *

Department of Molecular Pathology and Metabolic Disease, Faculty of Pharmaceutical Sciences, Tokyo University of Science, Yamazaki 2641, Noda, Chiba 278-0022, Japan

ARTICLE INFO

Article history:
Received 16 March 2012
Available online 23 March 2012

Keywords:
Nutlin3a
Nutlin3b
Caylin2
Poly(ADP-ribose) polymerase1
p53
MDM2
Proteasome

ABSTRACT

PARP1 is an important enzyme involved in various patho-physiological phenomena such as ischemia/reperfusion (I/R) injury, which occurs when blood flow is restored after cerebral infarction, myocardial infarction and transplantation of various organs. I/R-induced PARP1 over-activation is mediated by production of reactive oxygen species and is involved in NF-κB transactivation. For these reasons, PARP1 is an attractive target for strategies to protect against I/R injury. We previously reported that an MDM2 inhibitor Nutlin3a, a cis-imidazoline compound, induces PARP1 degradation in a p53 and proteasome-dependent manner. In this study, we evaluated the effect of Nutlin3a analogs, Nutlin3b and Caylin2, on PARP1 degradation. Like Nutlin3a, Caylin2, but not Nutlin3b, induced PARP1 degradation in both 3T3-L1 and 3T3-F442A. This result occurred almost in parallel with p53 accumulation. Furthermore Caylin2-induced PARP1 degradation was not observed in p53 deficient mouse embryonic fibroblasts or in the presence of the proteasome inhibitor MG132. These results suggest that Caylin2 induces PARP1 degradation by the same mechanism as Nutlin3a. Finally, we showed that Nutlin3a or Caylin2 treatment induces reversible PARP1 down-regulation without an inflammatory response. For protection against I/R injury, our results support the usability of the p53 inducible cis-imidazoline compounds, Nutlin3a and its analogs, as PARP1 inhibitors.

1. Introduction

Poly(ADP-ribosyl)ation, which is the post-translational protein modification, is involved in cell replication, DNA repair, cell death, and inflammation [1,2]. PARP1 is the most abundant PARP family member in cells, and is dramatically activated by DNA breaks. Therefore, massive DNA damage induces over-activation of PARP1, and then decreases ATP levels via over-consumption of cellular NAD^+, which is required for the ATP production in glycolysis and TCA cycle pathways. It has been also reported that PARP1 over-activation is involved in ischemia/reperfusion (I/R) injury, which occurs during the restoration of blood flow after cerebral infarction, myocardial infarction and organ transplantation [3–5]. For these reasons, PARP1 is an attractive target for protection against I/R injury [6].

We previously reported that Nutlin3a, an MDM2 ubiquitin ligase antagonist, induces p53 and proteasome-dependent PARP1 protein degradation [7]. It has been thought that Nutlin3a is a candidate for anti-tumor drugs, because MDM2 inhibition by Nutlin3a induces p53 stabilization, followed by p53-dependent apoptosis in tumor cells [8]. The discovery of Nutlin3a-induced PARP1 degradation prompted the use of Nutlin3a as a PARP1 inhibitor. Furthermore, considering that p53 has the potential to up-regulate anti-oxidant and anti-inflammatory genes [9–11], Nutlin3a may be a potent anti-I/R drug that has multiple points of action. However, the Nutlin3a pharmacophore that induce PARP1 protein degradation has not been identified. In the present study, to clarify whether Nutlin3a analogs were also able to induce PARP1 protein degradation in a manner similar to Nutlin3a, we examined the effect on PARP1 degradation by the commercially available Nutlin3a enantiomer, Nutlin3b [12,13], and by the Nutlin3a derivative, Caylin2 [14]. Furthermore, by using compounds possessing PARP1 degradation activity, we evaluated the reversibility of PARP1 degradation and the effect on anti-inflammatory IL6 gene expression.

2. Materials and methods

2.1. Cell culture and drugs

Mouse fibroblast 3T3-L1 and 3T3-F442A cell lines were purchased from the RIKEN Bioresource Center (Japan) and the European Collection of Animal Cell Cultures (UK), respectively. The cells were maintained in Dulbecco's modified Eagle's medium (DMEM, low glucose) (WAKO, Japan) with 10% fetal calf serum

* Corresponding authors. Fax: +81 4 7124 3676.
E-mail addresses: nokita7@rs.noda.tus.ac.jp (N. Okita), higami@rs.noda.tus.ac.jp (Y. Higami).
[1] These authors equally contributed to this work.

0006-291X/$ - see front matter © 2012 Elsevier Inc. All rights reserved.
http://dx.doi.org/10.1016/j.bbrc.2012.03.091

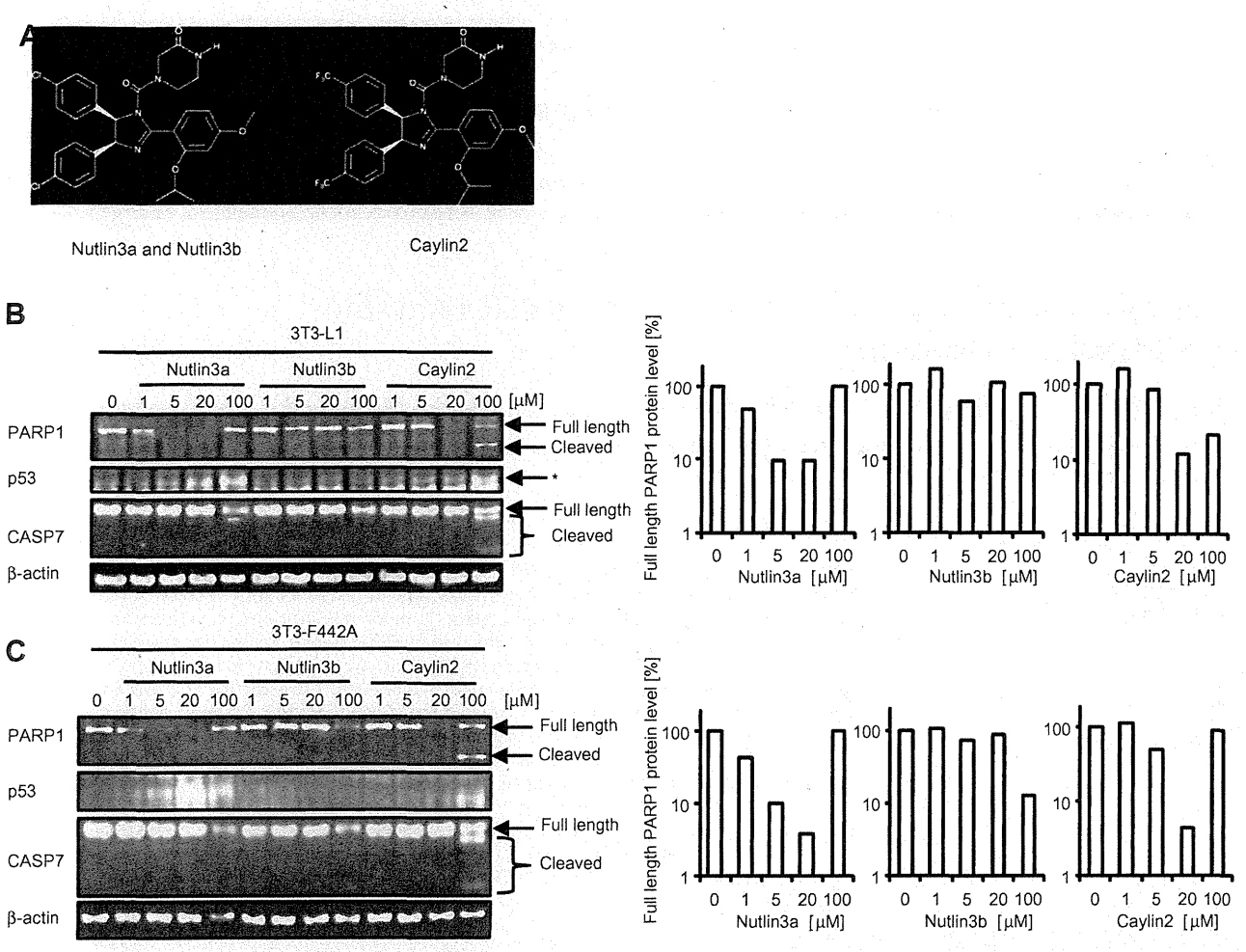

Fig. 1. Caylin2 but not Nutlin3b decreases in PARP1 protein levels in mouse fibroblasts. (A) Structures of Nutlin3a, Nutlin3b, and Caylin2. Mouse fibroblast 3T3-L1 (B) or 3T3-F442A (C) were treated with the indicated concentrations of Nutlin3a, Nutlin3b or Caylin2 for 8 h. The cell lysates were analyzed by Western blotting using the indicated antibodies (left pannel). Quantitative data are shown (right panel). In the p53 panel, the arrow and asterisk show the p53 and nonspecific bands, respectively. All experiments were performed at least three times, and representative data is shown.

and 1% penicillin/streptomycin (Sigma). p53+/+ or −/− MEFs were prepared as described previously [7]. The established MEFs were maintained in DMEM (high glucose) with 10% FCS, 0.1 mM 2-mercaptoethanol, and 1% penicillin/streptomycin. The proteasome inhibitor MG132 was purchased from WAKO (Japan). Nutlin3a, Nutlin3b, and Caylin2 were supplied by Cayman (USA).

2.2. Western blotting

Cell preparation and Western blotting were performed as described previously [7]. As primary antibodies, anti-PARP1 (clone C-2-10, WAKO, Japan), anti-p53 (clone Ab-1, Calbiochem, USA), anti-β actin (clone AC-15, SIGMA, USA), or anti-CASP7 (clone 1F3, MBL, Japan) antibodies were used. For secondary antibodies, horseradish peroxidase-conjugated $F(ab')_2$ fragment of goat anti-mouse IgG or anti-rabbit IgG (Jackson Immunoresearch, USA) were used. The specific proteins were visualized with ImmunoStar LD reagent (WAKO, Japan) and LAS3000 (Fuji Film, Japan), and the data were analyzed using MultiGauge software (Fuji Film, Japan).

2.3. RNA purification and RT-PCR

RNA purification and RT-PCR were performed using RNAiso PLUS, FastPure RNA kit, PrimeScript Reverse Transcriptase and random hexamers (all from TaKaRa, Japan) as described previously [7]. The PCR was performed using Platinum Taq DNA Polymerase High Fidelity (Invitrogen, USA) and primers for *TNFα* (forward, 5′-CCCTCACACTCAGATCATCTTCTC-3′; reverse, 5′-GCCTTGTCCCTTGAAGAGAACC-3′) *IL6* (forward, 5′-GCCTTCCCTACTTCACAAGTCC-3′; reverse, 5′-CAGAATTGCCATTGCACAAC-3′), or *TBP* (forward, 5′-CAGTACAGCAATCAACATCTCAGC-3′; reverse, 5′-CAAGTTTACAGCCAAGATTCACG-3′) as follows: initiation step, at 94 °C for 1 min; amplification step, at 94 °C for 1 min, at 60 °C for 15 s, at 68 °C for 15 s; termination step, 68 °C 15 s. PCR products were subjected to 1.8% agarose gel electrophoresis, stained with ethidium bromide, and visualized with LAS3000. The data was analyzed using MultiGauge software (Fuji Film, Japan).

3. Results

3.1. Caylin2. but not Nutlin3b induces a decrease in PARP1 protein levels in mouse fibroblast cell lines

Although we previously reported that Nutlin3a induces PARP1 protein degradation, we did not address whether Nutlin3a analogs also have the potential to induce PARP1 degradation [7]. Here, we investigated the inducibility of PARP1 degradation by two such analogs, Nutlin3b and Caylin2 in mouse fibroblast cell lines

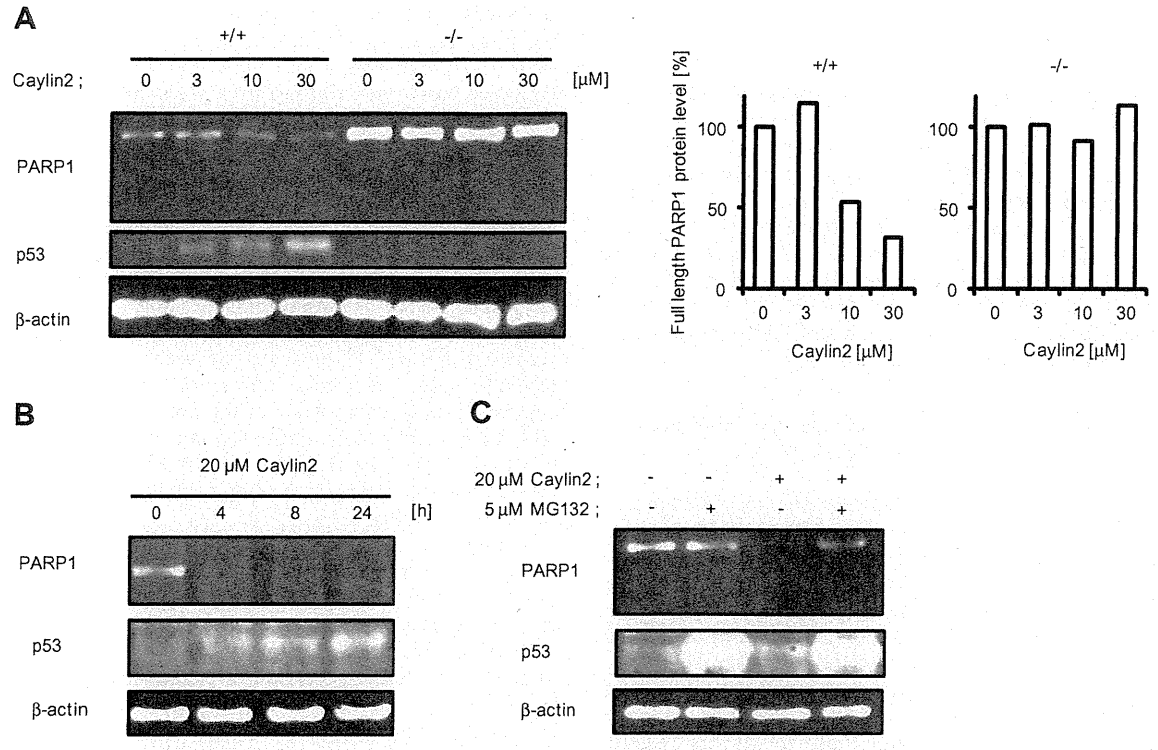

Fig. 2. Caylin2-induced PARP1 degradation is p53 status and proteasome-dependent. (A) p53+/+ and p53−/− MEFs were treated with the indicated concentrations of Caylin2 for 8 h. Cell lysates were analyzed by Western blotting using the indicated antibodies (left panel). Quantitative data are shown (right panel). Each 2 to 3 clones of p53+/+ and p53−/− MEFs were analyzed and representative data are shown. (B) 3T3-L1 cells were treated with 20 μM Caylin2 for the indicated times. The proteins were subjected to Western blotting. (C) 3T3-L1 cells were treated with 20 μM Caylin2 in the presence or absence of 5 μM MG132 proteasome inhibitor (MG) for 8 h, and cell lysates were then subjected to Western blotting using the indicated antibodies.

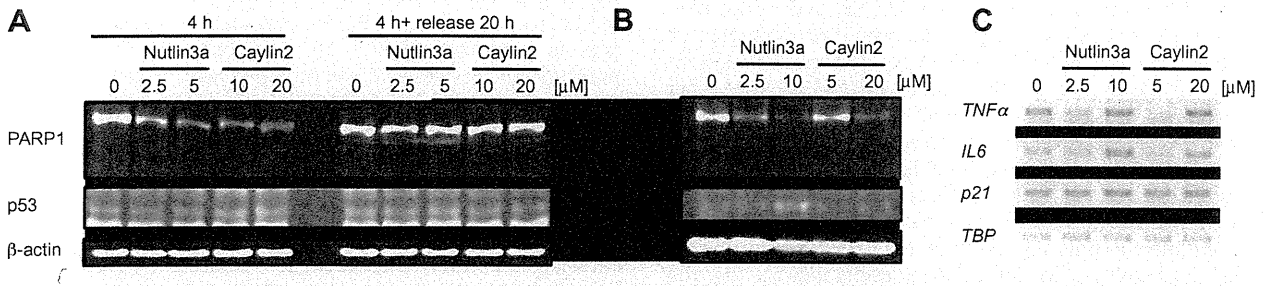

Fig. 3. Nutlin3a or Caylin2 treatment induces reversible PARP1 down-regulation without an inflammatory response. (A) 3T3-L1 cells were treated with Nutlin3a (2.5 or 5 μM) or Caylin2 (10 or 20 μM) for 4 h. After these treatments, cells were also cultured in normal growth medium without treatment for a further 20 h. The cell lysates were analyzed by Western blotting using the indicated antibodies. (B, C) 3T3-L1 cells were treated with 2.5 μM Nutlin3a or 5 μM Caylin2 for 4 h. The protein and RNA expression were analyzed by Western blotting (B) or RT-PCR (C).

(Fig. 1). Nutlin3b is an inactive enantiomer of Nutlin3a, whereas Caylin2 is a Nutlin3a derivative in which trifluoromethyl groups are substituted for chlorine on the 2 phenyl rings (Fig. 1A) [8,12]. As shown in Fig. 1B and C, for both cell lines, 1–20 μM Nutlin3a treatment markedly decreased PARP1 protein levels in a dose dependent manner, whereas 100 μM Nutlin3a treatment had no effect, as per our previous report. p53 accumulation was dose dependent, increasing with the concentration range. Additionally, after 100 μM Nutlin3a-treated, both cell lines were detached from the culture dish and appeared to die without significant CASP7 activation. This observation was consistent with our previous data [7]. Nutlin3b treatment did not markedly alter p53 protein levels in either cell line. In 3T3-L1 cells, Nutlin3b treatment did not affect PARP1 protein level (Fig. 1B). On the other hand, in 3T3-F442A cells, only 100 μM Nutlin3b treatment decreased the PARP1 protein level (Fig. 1C). Similar to the Nutlin3a treatment, 100 μM Nutlin3b-treated cells seemed to die without significant CASP7 activation. Interestingly, Caylin2 treatment showed a signature profile of PARP1 protein in both cell lines. 20 μM Caylin2 treatment induced a significant decrease in PARP1 protein and 100 μM Caylin2 treatment induced PARP1 cleavage, which is considered as an apoptotic hallmark as well as activation of apoptotic caspases such as CASP2, 3, 6, 7, 9, and 10 [15–17]. Indeed, a trypan blue exclusion assay showed that Caylin2-treated cells were viable at 20 μM and dead at 100 μM (Supplemental Fig. 1).

3.2. PARP1 down-regulation by Caylin2 treatment is p53 and proteasome-dependent

Since we previously reported that Nutlin3a-induced PARP1 degradation occurs in a p53 and proteasome dependent manner, we sought to confirm using the same methods as our previous report whether Caylin2-induced PARP1 degradation is inhibited by p53 depletion or proteasome inhibition. As shown in Fig. 2A, p53 WT MEFs, but not p53 KO MEFs, displayed decreasing PARP1 protein levels in a Caylin2 dose dependent manner. Furthermore, as shown in Fig. 2B, Caylin2-induced PARP1 degradation was inhibited by co-treatment with the proteasome inhibitor MG132. These results indicate that Caylin2, like Nutlin3a, induces PARP1 degradation in a p53 and proteasome-dependent manner.

3.3. Nutlin3a or Caylin2 treatment induces reversible PARP1 down-regulation without an inflammatory response

Since PARP1 plays roles in the maintenance of cellular homeostasis through various signal transduction pathways [1,2], reversible down-regulation of the PARP1 protein level is important to protect tissues from I/R injury. Therefore we investigated the reversibility of Nutlin3a- or Caylin2-induced PARP1 degradation. 3T3-L1 cells were treated with Nutlin3a (2.5 or 5 μM) or Caylin2 (10 or 20 μM) for 4 h, and then cultured for 20 h. After 4 h of Nutlin3a or Caylin2 treatment (transient treatment), PARP1 protein levels decreased, although p53 protein levels were not markedly altered (Fig. 3A). After release from those treatments (+20 h), PARP1 protein levels were recovered (Fig. 3A). These results show that Nutlin3a or Caylin2-induced PARP1 degradation is reversible. As it has been reported that Nutlin3a-induced p53 activation leads to up-regulation of inflammatory cytokines [18], we also investigated the influence on inflammation by the transient Nutlin3a or Caylin2 treatment (Fig. 3B). 3T3-L1 cells were treated with the indicated doses of Nutlin3a or Caylin2 for 4 h, and then analyzed the TNFα and IL6 inflammatory genes by RT-PCR. Under these conditions, Nutlin3a or Caylin2 treatment induced PARP1 degradation in a dose dependent manner. Interestingly, we observed different inflammatory responses under these condition (Fig. 3C). The higher dose treatments of Nutlin3a or Caylin2 significantly induced IL6 mRNA expression. However, these doses had little effect or only slightly induced TNFα mRNA expression. On the other hand, the lower dose treatments of Nutlin3a or Caylin2, which were capable of inducing PARP1 degradation, inhibited TNFα mRNA expression and did not affect or only slightly inhibited IL6 mRNA expression. Taken together with Fig. 3B and C, these results indicate that the lower dose treatment of Nutlin3a or Caylin2 has the potential to induce PARP1 degradation without inducing an inflammatory response.

4. Discussion

In this study, we examined the effect of treatment by Nutlin3a analogs on PARP1 protein levels. We demonstrated that Caylin2 induces PARP1 degradation in a similar manner to Nutlin3a. Taken together with our previous study, these results indicate that p53-inducible cis-imidazoline compounds have the potential to induce PARP1 degradation. In the context of using Nutlin3a, Caylin2 and related derivatives as "PARP1 degradation inducers" for I/R injury therapy, a major advantage of this study is that it has demonstrated that Nutlin3a- or Caylin2-induced PARP1 degradation is reversible (Fig. 3A). I/R injury is the tissue damage that occurs during the ischemic and reperfusion period, and as such commonly occurs as a result of ischemic infarction and its treatment or during organ transplantation. In the injured tissues, PARP1 is over-activated by reactive oxygen-mediated DNA damage, resulting in decreases in ATP levels via over-consumption of cellular NAD^+ [1,2]. Therefore, PARP1 inhibition has protective effects on I/R injury. Furthermore, PARP1 itself plays roles in the maintenance of cellular homeostasis through its involvement in the regulation of various signal transduction pathways [1,2]. Taken together, transient PARP1 degradation is valuable in regard to both protection from I/R injury and to allowing for a quick recovery from the harmful effects of PARP1 inhibition. There have been some previous reports of IL6 regulation by p53 or PARP1. p53 has been reported to repress not only IL6 but also the promoter activity of NF-κB, a transcriptional factor of various inflammatory genes including IL6 [10,11]. Additionally, PARP1 activation inhibits the DNA-binding activity of NF-κB [19]. In this study, we showed that Nutlin3a or Caylin2 causes differential effects on inflammatory responses depending on the magnitude of the doses used (Fig. 3C). Our results suggest that the choice of appropriate doses and timing of treatments would be critical to obtain only the beneficial effects on PARP1 degradation when using Nutlin3a or Caylin2 for protection from I/R injury.

Recently, it was reported that inflammasome activation of cardiac fibroblasts is essential for myocardial I/R [20]. So far, our work has revealed that the PARP1 degradation pathway functions efficiently in fibroblast cell lines [7]. These findings support the possibility of practical use of this PARP1 degradation pathway. Further research will require several lines of investigation. Firstly, it will be interesting to identifiy the stereocenter that specifically induces PARP1 degradation. The chiral separation of Nutlin3 (Nutlin3a and Nutlin3b) has been achieved, although the absolute stereocenter has not been known [12,13]. In Caylin2 the chiral separation has not been achieved. We predict that Caylin2a (Caylin2 of Nutlin3a type), but not Caylin2b (Caylin2 of Nutlin3b type), may be the potential to induce PARP1 degradation and are performing further analyses now. Secondly, it will be important to explore PARP1 degradation inducers that different structures than the cis-imidazoline compounds such as Nutlin3a or Caylin2. Thus, elucidation of the mechanism of reversible PARP1 degradation induction is important for the optimization of compounds which induce this phenomenon, resulting in the establishment of selective chemotherapeutic strategies against I/R injury.

Acknowledgments

The authors thank Dr. Susumu Kobayashi (Tokyo University of Science, Japan) and Dr. Takahiro Suzuki (Tokyo University of Science, Japan) for their valuable expertise and all members of Higami laboratory for their cooperation. This work was supported by Grant-in-Aid for Young Scientists (B) from the Ministry of Education, Culture, Sports, Science and Technology (23790201) (N.O.) and partially by Challenging Exploratory Research from the Ministry of Education, Culture, Sports, Science and Technology (23659207) (Y.H.). RIDAI SCITEC holds a patent (PCT/JP2012/052565) on the method of treating ischemia/reperfusion injury, and N.O., and Y.H. are the inventors of the patent.

References

[1] M. Masutani, H. Nakagama, T. Sugimura, Poly(ADP-ribosyl)ation in relation to cancer and autoimmune disease, Cell. Mol. Life Sci. 62 (2005) 769–783.
[2] M. Miwa, M. Masutani, PolyADP-ribosylation and cancer, Cancer Sci. 98 (2007) 1528–1535.
[3] H.K. Eltzschig, T. Eckle, Ischemia and reperfusion – from mechanism to translation, Nat. Med. 17 (2011) 1391–1401.
[4] S.J. van Wijk, G.J. Hageman, Poly(ADP-ribose) polymerase-1 mediated caspase-independent cell death after ischemia/reperfusion, Free Radic. Biol. Med. 39 (2005) 81–90.
[5] P. Pacher, C. Szabo, Role of the peroxynitrite-poly(ADP-ribose) polymerase pathway in human disease, Am. J. Pathol. 173 (2008) 2–13.

[6] D.V. Ferraris, Evolution of poly(ADP-ribose) polymerase-1 (PARP-1) inhibitors, from concept to clinic, J. Med. Chem. 53 (2010) 4561–4584.
[7] S. Matsushima, N. Okita, M. Oku, W. Nagai, M. Kobayashi, Y. Higami, An Mdm2 antagonist, Nutlin-3a, induces p53-dependent and proteasome-mediated poly(ADP-ribose) polymerase1 degradation in mouse fibroblasts, Biochem. Biophys. Res. Commun. 407 (2011) 557–561.
[8] L.T. Vassilev, B.T. Vu, B. Graves, D. Carvajal, F. Podlaski, Z. Filipovic, N. Kong, U. Kammlott, C. Lukacs, C. Klein, N. Fotouhi, E.A. Liu, In vivo activation of the p53 pathway by small-molecule antagonists of MDM2, Science 303 (2004) 844–848.
[9] A.A. Sablina, A.V. Budanov, G.V. Ilyinskaya, L.S. Agapova, J.E. Kravchenko, P.M. Chumakov, The antioxidant function of the p53 tumor suppressor, Nat. Med. 11 (2005) 1306–1313.
[10] U. Santhanam, A. Ray, P.B. Sehgal, Repression of the interleukin 6 gene promoter by p53 and the retinoblastoma susceptibility gene product, Proc. Natl. Acad. Sci. USA 88 (1991) 7605–7609.
[11] E.A. Komarova, V. Krivokrysenko, K. Wang, N. Neznanov, M.V. Chernov, P.G. Komarov, M.L. Brennan, T.V. Golovkina, O.W. Rokhlin, D.V. Kuprash, S.A. Nedospasov, S.L. Hazen, E. Feinstein, A.V. Gudkov, p53 is a suppressor of inflammatory response in mice, FASEB J. 19 (2005) 1030–1032.
[12] Z. Wang, M. Jonca, T. Lambros, S. Ferguson, R. Goodnow, Exploration of liquid and supercritical fluid chromatographic chiral separation and purification of Nutlin-3 – a small molecule antagonist of MDM2, J. Pharm. Biomed. Anal. 45 (2007) 720–729.
[13] Cayman Chemical, http://www.caymanchem.com/app/template/Product.vm/catalog/10009816.
[14] Cayman Chemical, http://www.caymanchem.com/app/template/Product.vm/catalog/10005002.
[15] S.H. Kaufmann, S. Desnoyers, Y. Ottaviano, N.E. Davidson, G.G. Poirier, Specific proteolytic cleavage of poly(ADP-ribose) polymerase: an early marker of chemotherapy-induced apoptosis, Cancer Res. 53 (1993) 3976–3985.
[16] Y.A. Lazebnik, S.H. Kaufmann, S. Desnoyers, G.G. Poirier, W.C. Earnshaw, Cleavage of poly(ADP-ribose) polymerase by a proteinase with properties like ICE, Nature 371 (1994) 346–347.
[17] C. Pop, G.S. Salvesen, Human caspases: activation, specificity, and regulation, J. Biol. Chem. 284 (2009) 21777–21781.
[18] B. Huang, D. Deo, M. Xia, L.T. Vassilev, Pharmacologic p53 activation blocks cell cycle progression but fails to induce senescence in epithelial cancer cells, Mol. Cancer Res. 7 (2009) 1497–1509.
[19] W.J. Chang, R. Alvarez-Gonzalez, The sequence-specific DNA binding of NF-kappa B is reversibly regulated by the automodification reaction of poly(ADP-ribose) polymerase 1, J. Biol. Chem. 276 (2001) 47664–47670.
[20] M. Kawaguchi, M. Takahashi, T. Hata, Y. Kashima, F. Usui, H. Morimoto, A. Izawa, Y. Takahashi, J. Masumoto, J. Koyama, M. Hongo, T. Noda, J. Nakayama, J. Sagara, S. Taniguchi, U. Ikeda, Inflammasome activation of cardiac fibroblasts is essential for myocardial ischemia/reperfusion injury, Circulation 123 (2011) 594–604.

Mechanisms of Ageing and Development 133 (2012) 255–266

Contents lists available at SciVerse ScienceDirect

Mechanisms of Ageing and Development

journal homepage: www.elsevier.com/locate/mechagedev

Differential responses of white adipose tissue and brown adipose tissue to caloric restriction in rats

Naoyuki Okita [a,1], Yusuke Hayashida [a,1], Yumiko Kojima [a,1], Mayumi Fukushima [a], Keiko Yuguchi [a], Kentaro Mikami [a], Akiko Yamauchi [a], Kyoko Watanabe [a], Miturn Noguchi [b], Megumi Nakamura [c], Toshifusa Toda [c], Yoshikazu Higami [a,*]

[a] Molecular Pathology & Metabolic Disease, Faculty of Pharmaceutical Sciences, Tokyo University of Science, Tokyo, Japan
[b] Department of Urology, Faculty of Medicine, Saga University, Japan
[c] TMIG Proteomics Collaboration Center, Tokyo Metropolitan Institute of Gerontology, Tokyo, Japan

ARTICLE INFO

Article history:
Received 30 August 2011
Received in revised form 14 December 2011
Accepted 22 February 2012
Available online 10 March 2012

Keywords:
Caloric restriction
Adipose tissue
Proteome analysis
Mitochondrial biogenesis
Fatty acid biosynthesis
Mitochondrial biogenesis

ABSTRACT

Caloric restriction (CR) slows the aging process and extends longevity, but the exact underlying mechanisms remain debatable. It has recently been suggested that the beneficial action of CR may be mediated in part by adipose tissue remodeling. Mammals have two types of adipose tissue: white adipose tissue (WAT) and brown adipose tissue (BAT). In this study, proteome analysis using two-dimensional gel electrophoresis combined with MALDI-TOF MS, and subsequent analyses were performed on both WAT and BAT from 9-month-old male rats fed *ad libitum* or subjected to CR for 6 months. Our findings suggest that CR activates mitochondrial energy metabolism and fatty acid biosynthesis in WAT. It is likely that in CR animals WAT functions as an energy transducer from glucose to energy-dense lipid. In contrast, in BAT CR either had no effect on, or down-regulated, the mitochondrial electron transport chain, but enhanced fatty acid biosynthesis. This suggests that in CR animals BAT may change its function from an energy consuming system to an energy reservoir system. Based on our findings, we conclude that WAT and BAT cooperate to use energy effectively *via* a differential response of mitochondrial function to CR.

1. Introduction

Mammals have two types of adipose tissue, white adipose tissue (WAT) and brown adipose tissue (BAT), which can be distinguished by their morphology and function (Saely et al., 2010). WAT is a major tissue for energy storage in the form of triglycerides (TG). It consists predominantly of white adipocytes that store energy in TG-containing unilocular droplets. Several WAT-derived secretory molecules (adipokines), such as adiponectin, leptin and pro-inflammatory cytokines including tumor necrosis factor α (TNFα), have been characterized. Adiponectin enhances insulin sensitivity and fatty acid oxidation *via* the cellular fuel sensor AMP-activated protein kinase (AMPK). Moreover, it acts as an anti-inflammatory and anti-atherogenic adipokine (Stofkova, 2009; Yamauchi et al., 2001, 2002). Leptin reduces appetite and enhances energy expenditure *via* the hypothalamus/sympathetic nervous system, and also functions as a pro-inflammatory adipokine (Stofkova, 2009). TNFα promotes insulin resistance (Hotamisligil et al., 1995). Thus, several adipokines are involved in energy homeostasis, insulin resistance and inflammation (Gnacińska et al., 2009; Torres-Leal et al., 2010). It is well known that white adipocytes alter their characteristics with their size. Large hypertrophic adipocytes, possessing more TG, secrete less adiponectin and more pro-inflammatory cytokines including leptin, while small adipocytes, which have less TG, secrete more adiponectin and less pro-inflammatory adipokines (DeClercq et al., 2008). Moreover, small adipocytes are generally found to be more sensitive to insulin and act as powerful buffers, absorbing lipids in the postprandial period. If this buffering action is impaired, extra adipose tissues can accumulate lipids in the form of TG, resulting in insulin resistance (Frayn, 2002). Small adipocytes are therefore considered more beneficial for a healthy lifespan than large ones (Higami et al., 2005; Zhu et al., 2007).

In contrast to WAT, BAT plays an important role in energy expenditure. It predominantly consists of mitochondria-rich brown adipocytes, which have multilocular lipid droplets and express the BAT-specific mitochondrial protein, Uncoupling Protein 1 (UCP1; Farmer, 2008; Saely et al., 2010). UCP1 uncouples mitochondrial ATP synthesis from electron transport chain

* Corresponding author at: Molecular Pathology & Metabolic Disease, Faculty of Pharmaceutical Sciences, Tokyo University of Science, 2641 Yamazaki, Noda, Chiba 278-8510, Japan. Tel.: +81 4 7121 3676; fax: +81 4 7121 3676.
E-mail address: higami@rs.noda.tus.ac.jp (Y. Higami).
[1] These authors contributed equally to this work.

0047-6374/$ – see front matter © 2012 Elsevier Ireland Ltd. All rights reserved.
doi:10.1016/j.mad.2012.02.003

activity, and is responsible for energy expenditure *via* heat production. BAT is highly vascularized and innervated by the sympathetic nervous system. It is a major site of both cold- and diet-induced thermogenesis, particularly in small rodents (Farmer, 2008; Saely et al., 2010). Recent studies using positron-emission tomography have identified BAT in human adults, and shown that its activity correlates inversely with body mass index. Active BAT therefore appears to play an important role in the control of body temperature and adiposity in humans (Saely et al., 2010).

Recently, new genetic interventions that extend mammalian lifespan have emerged (Kenyon, 2005). Caloric restriction (CR), however, remains the most robust, reproducible and simple experimental manipulation known to extend both median and maximum lifespan, and to retard several age-related pathophysiological changes in laboratory rodents (Masoro, 2005; Sinclair, 2005; Weindruch and Walford, 1988; Yu, 1994). The anti-aging and/or pro-longevity effects of CR have been observed in several species, from yeast to laboratory rodents (Masoro, 2005; Sinclair, 2005). Recent studies suggest that CR is effective in non-human primates as well (Colman et al., 2009). It is widely accepted that suppression of the growth hormone (GH)/insulin-like growth factor (IGF-1) signal, attenuation of oxidative and other stresses, modulation of glycemia and insulinemia, enhanced mitochondrial biogenesis and activation of sirtuins may be significant factors in the actions of CR, but the exact underlying mechanisms are still debatable (Masoro, 2005; Sinclair, 2005). It has been reported that fat-specific insulin receptor knockout (FIRKO) mice live longer than their controls (Blüher et al., 2003). These mice reduce adiposity and enhance mitochondrial biogenesis with altered secretion of adipokines, including higher adiponectin and lower pro-inflammatory cytokines (Blüher et al., 2002; Katic et al., 2007). The transcription factors C/EBPα, C/EBPβ and peroxisome proliferator-activated receptor γ (PPARγ) are master regulators of adipocyte differentiation (Farmer, 2006). Mice in which C/EBPα was replaced with C/EBPβ (β/β mice) live longer and have reduced adiposity (Chiu et al., 2004). In contrast, the hetero-deficiency PPARγ knockout (KO) mice have a shorter lifespan (Argmann et al., 2009). Transgenic mice expressing adiponectin in the liver live longer than controls and show reduced high-calorie diet-induced obesity (Otabe et al., 2007). These results show that altered gene expression in the adipose tissue, and modulation of adipokine secretion, can influence the lifespan of rodents. CR reduces adiposity by altering the gene expression profile (Higami et al., 2004, 2006a), and lowering plasma insulin and leptin levels, as well as raising plasma adiponectin levels (Yamaza et al., 2007; Zhu et al., 2007). CR also reverses age-associated insulin resistance, possibly through decreased adiposity (Barzilai et al., 1998). Moreover, in mice, CR promotes mitochondrial biogenesis in both WAT and BAT, and it has been suggested that PPARγ co-activator 1α (PGC1α), Sirt1 and Sirt3 are key players in CR-enhanced mitochondrial biogenesis (Anderson and Prolla, 2009; Nisoli et al., 2005; Shi et al., 2005). Therefore, we hypothesized that the beneficial actions of CR may be partially mediated by functional alteration of WAT and BAT. Proteome analysis of WAT from 24-month-old rats fed *ad libitum* (AL) or subjected to CR was recently reported (Valle et al., 2010). However, to our knowledge analysis of the effects of CR in both WAT and BAT at a young age, and a comparison of these effects, has not yet been reported.

In this study, to understand the molecular basis of CR-associated metabolic alterations in adipose tissues, we performed histological examination and proteome analysis of both WAT and BAT from 9-month-old male rats fed AL or subjected to CR for 6 months, and the responses to CR were compared between WAT and BAT. This enabled differential and similar responses to CR between both tissues to be identified.

2. Materials and methods

2.1. Animals and diet

The present study was conducted in accordance with the provisions of the Ethics Review Committee for Animal Experimentation at Tokyo University of Science. Male Wistar rats aged 5–7 weeks were purchased from Clea Inc. (Tokyo, Japan) and were maintained under SPF conditions at 23 °C and a 12 h light–dark cycle, in the Laboratory Animal Center at the Faculty of Pharmaceutical Sciences, Tokyo University of Science. All rats were provided with water and fed *ad libitum* with a Labo MR Stock diet (NOSAN, Yokohama, Japan).

From 12 weeks of age, rats were divided into two groups: one was fed *ad libitum* (AL) and the other was calorie restricted (CR, 70% of the *ad libitum* energy intake). CR rats were fed every other day (Higami et al., 2006b). Their 2-day food allotment was equal to 140% of the mean daily intake of AL rats. At 9 months of age, all rats were sacrificed under anesthesia with isoflurane inhalation (Mylan, Canonsburg, PA, USA) 3–5 h after turning on the lights. Prior to sacrifice, CR and AL groups were further divided into two treatments (fed or fasted) as follows. CR-fed rats were provided with food 30 min prior to turning off the lights in the evening, and were sacrificed the following morning. CR-fasted rats were fasted overnight for approximately 16 h prior to sacrifice. To evaluate the effect of fasting, half of the AL rats were sacrificed 16 h after the removal of food, which occurred when the lights were turned off (AL-fasted), while the other half were sacrificed without removing the food (AL-fed). Mean body weight data (±SEM) of AL-fasted and CR-fasted rats are shown in Table 1. When the animals were sacrificed, both epididymal WAT and interscapular BAT were collected and their weights measured (Table 1). A sub-sample of the isolated WAT and BAT were fixed in a buffered formalin solution for histological examination, and the rest was immediately diced, frozen in liquid nitrogen, and stored at −80 °C.

2.2. Histological examination

Fixed tissues were processed routinely, embedded in paraffin, and sectioned. 5 μm sections were stained with hematoxylin–eosin. Stained sections were scanned by microscopy with a CCD camera (Nikon, Tokyo, Japan). The size distribution of each white area in the black-and-white images, which indicates a lipid droplet, was measured and calculated using "ImageJ 1.43u/Java1.6.0_22" software. To avoid inter-rating variation, a single observer (Yu. H.) carried out the morphometric analysis.

2.3. Analysis of triglyceride (TG) contents

Total lipid was extracted from WAT and BAT of AL-fasted and CR-fasted rats, and the triglyceride (TG) content was measured using a LabAssay™ Triglyceride kit (Wako, Osaka, Japan), according to a previous report (Higami et al., 2006a) and the manufacturer's instructions. The TG content per 100 mg protein was calculated.

2.4. Two-dimensional gel electrophoresis (2-DE)

Two-dimensional gel electrophoresis (2-DE) using the IPG-DALT system and subsequent MALDI-TOF MS analysis were performed as previously described (Nakamura et al., 2006). Briefly, to extract total protein, frozen WAT and BAT from AL-fed, AL-fasted, CR-fed and CR-fasted rats were homogenized in extraction buffer containing 5 M urea, 2 M thiourea, 2% (w/v) 3-[(3-cholamidopropyl) dimethylammonio]-1-propanesulfonate (CHAPS), 2% (w/v) sulfobetaine10, 2% Pharmalyte 3-10, 65 mM dithiothreitol (DTT), 1% protease inhibitor cocktail and 1% phosphatase inhibitor cocktail, using a sonicator. Samples were centrifuged at 15,000 rpm, at 20 °C for 30 min, and the supernatants were collected. The supernatant samples were prepared from six animals in each group, and each individual was assessed separately. The protein content of each sample was determined using the Bradford method.

First-dimensional isoelectric focusing (IEF) was carried out on nonlinear immobilized pH gradients (Immobiline DryStrip, pH 3–10 NL, 18 cm long; GE Healthcare, Cleveland, OH, USA). Passive sample application during rehydration was performed by placing the Immobiline DryStrip gel side down overnight in a rehydration tray that contained the sample in the rehydration solution (6 M urea, 2 M thiourea, 13 mM DTT, 1% Pharmalyte 3-10, 2.5 mM acetic acid, 0.0025% Orange G and 2% Triton X-100). As the strip hydrates, proteins in the sample are absorbed

Table 1
Body and tissue weights of rats.

	AL	CR
Body weight (g)	523 ± 11	344 ± 9*
WAT weight (g)	7.04 ± 0.464	2.16 ± 0.160*
WAT weight/body weight (%)	1.34 ± 0.078	0.627 ± 0.044*
BAT weight (g)	0.454 ± 0.036	0.255 ± 0.014*
BAT weight/body weight (%)	0.087 ± 0.007	0.074 ± 0.005

* $p < 0.001$ by Student's *t*-test.

and distributed over the entire length of the strip. The IEF was performed at 20 °C starting at 500 V, with the voltage being gradually increased to 3500 V, using a PowerPhoreStar power supply (Anatech, Tokyo, Japan). After electrofocusing, the gel strips were equilibrated for 45 min with gentle shaking in 5 mL of equilibration buffer (6 M urea, 32 mM DTT, 25 mM Tris–HCl, pH 6.8, 2% SDS, 0.0025% BPB and 30% glycerol). In the second-dimension SDS–PAGE, the equilibrated gel strips were placed on top of 7.5% polyacrylamide gels (18 cm × 20 cm × 1 mm), and run in SDS running buffer (0.1 M Tris, 0.1 M Tricine and 0.1% SDS) until the dye front reached the bottom of the gel. Then, the gel was fixed with fixing solution (10% acetic acid and 50% methanol) and washed with washing solution (7% acetic acid and 10% methanol). Finally, the gel was stained with SYPRO Ruby Protein Gel Stain (Molecular Probe, Eugene, OR, USA) and washed with washing solution (8% acetic acid and 10% methanol) and pure water.

Fluorescent gel images were obtained by scanning with a FluoroPhoreStar 3000 (Anatech) and analyzed with Progenesis PG200 software (Nonlinear Dynamics, Durham, NC, USA). Molecular masses were determined by running standard protein markers, covering the range of 10–250 kDa. The *pI* values used were those given by the supplier of the IPG strips. After background subtraction, spots from each gel were automatically matched to the spots on a reference gel. To validate automated spot detection and matching, images were edited manually and streaks, speckles and artifacts were removed. The reference gel was obtained using mixed samples from AL-fed and CR-fed rat tissues. For all spot-intensity calculations, normalization volumes were used to calculate relative intensity (RI) for each spot: RI = vi/vt, where vi is the volume (pixel intensities integrated over the area of each spot) of the individual spot, and vt is the sum of the volumes of all matched spots. Only spots displaying a significant change (≥1.4-fold) in their normalized spot intensity were considered for protein identification.

2.5. Matrix-assisted laser desorption/ionization time-of-flight mass spectrometry (MALDI-TOF MS) analysis

For mass spectrometric identification, protein spots on the SYPRO Ruby-stained 2-DE gel were excited and the spots that showed different density were excised with a FluoroPhoreStar3000 gel picker (Anatech). The gel pieces were reduced with 1.5 mg/mL DTT in 100 mM ammonium bicarbonate, alkylated with 10 mg/mL iodoacetamide in 100 mM ammonium bicarbonate, then destained, washed, and finally dried. Subsequently, the gel pieces were digested with 5 μg/mL sequencing grade modified trypsin (Promega, Madison, WI, USA) in a 50 mM ammonium bicarbonate and 30% acetonitrile solution, at 30 °C overnight. The tryptic peptide mixture samples were concentrated in a SpeedVac Vacuum system (Savant Instruments, Holbrook, NY, USA) and were rehydrated with 10 μL of 0.1% trifluoroacetic acid (TFA). The samples were then adsorbed onto a Zip-Tip μC18 column (Millipore, Billerica, MA, USA). The resin was washed with 0.1% TFA and the peptides were eluted with 50% acetonitrile in 0.1% TFA. The elution was analyzed by the peptide mass fingerprint (PMF) method, based on MALDI-TOF MS as follows: 2 μL of tryptic peptides were spotted onto a ready-to-use Shimadzu 384 target plate (Shimadzu, Kyoto, Japan), and mixed with 0.5 μL of matrix solution [53 mM CHCA (α-cyano-4-hydroxycinnamic acid), 50% acetonitrile, 40% methanol and 0.1% TFA]. Mass spectra were collected on an AXIMA-CFR MALDI-TOF instrument (Shimadzu) in reflectron positive ion mode. The instrument was externally calibrated using the calibrant spots on the pre-spotted target. Monoisotopic peaks were generated by Kompact software (Shimadzu), and protein identification was carried out primarily using the PMF Search of Mascot (http://www.matrixscience.com) and the MS-Fit search engine in Protein Prospector (http://prospector.ucsf.edu) by sending a query of the PMF peak list. In some cases, samples were further analyzed by MALDI TOF TOF MS/MS (AXIMA-TOF2; Shimadzu). An MS/MS ion search of Mascot was used for confirmation.

2.6. DNA extraction

Total DNA, including mitochondrial DNA (mtDNA), was extracted from WAT and BAT by digestion with proteinase K and 10% SDS (100 μg/μL) in a buffer containing 150 mM NaCl, 10 mM Tris–HCl, pH 8.0, and 10 mM EDTA. Homogenate samples were incubated overnight at 55 °C, and then an equal volume of phenol was added and samples were rotated for 1 h. After centrifugation, the aqueous phase was removed to a fresh tube and rotated with an equal volume of PCI (phenol/chloroform/isoamyl alcohol) for 1 h. To remove RNA, the aqueous phase was incubated with 0.02 volume of RNase A (Wako, Osaka, Japan) for 1 h at 37 °C. This phenol and PCI procedure was repeated once more. DNA was precipitated from the aqueous phase by adding 0.1 volume of 3 M sodium acetate after adding a double volume of 100% ethanol. The DNA was washed twice with 180 μL of 70% ethanol, air dried gently and re-suspended in TE buffer. The concentration was adjusted to 20 ng/μL.

2.7. Analysis of mtDNA contents

A quantitative PCR assay was performed using the Applied Biosystems 7300 real-time PCR system (Life Technologies, Carlsbad, CA, USA) (Koekemoer et al., 1998). Nuclear DNA and mtDNA were amplified by real-time PCR for solute carrier family 16, member 1 (SLC16A1) and cytochrome c oxidase subunit 2 (COX2), respectively. The primer pairs' sequences for real-time PCR analysis of SLC16A1 and COX2 were: SLC16A1 (forward) 5′-TAG CTG GAT CCC TGA TGC GA-3′, (reverse) 5′-GCA TCA GAC TTC CCA GCT TCC-3′ (32); COX2 (forward) 5′-CTT ACA AGA CGC CAC ATC AC-3′, (reverse) 5′-GAA TTC GTA GGG AGG GAA GG-3′ (Jahnke et al., 2010). Relative amounts of mtDNA were expressed as COX2/SLC16A1.

2.8. Analysis of mitochondrial activities

Activities of citrate synthase (CS) and electron transport chain complex IV, cytochrome c oxidase (Complex IV), were measured as previously reported with some modifications (Alp et al., 1976; Daley et al., 2005). Briefly, WAT and BAT were homogenized in homogenization buffer containing 50 mM Tris–HCl, pH 7.4, 150 mM NaCl, 1% phosphatase inhibitor cocktail, 5 mM EDTA, 1% protease inhibitor cocktail, 1% Triton X-100 and 0.05% sodium deoxycholate. Protein concentration was determined using the BCA protein assay kit (Thermo Scientific, Rockford, IL, USA) according to the manufacturer's protocol.

For CS activity measurements, a reaction mixture containing 0.1 mM 5,5-dithiobis-(2-nitrobenzoic) acid (Wako), 0.5 mM acetyl-CoA (Wako), 0.1% Triton X-100 and 100 mM Tris–HCl, pH 8.0, with the tissue homogenate was prepared. The homogenates contained 5–8 μg protein from WAT or 0.5–0.8 μg protein from BAT. After incubation at 28 °C for 5 min, the absorbance at 412 nm (SpectraMax Plus384, Molecular Devices, Sunnyvale, CA, USA) was measured for 3 min to determine the nonspecific activity. Reactions were then initiated by addition of 0.5 mM oxaloacetate (Wako) in a final volume of 200 μL, and the change in absorbance was recorded for at least 3 min (Alp et al., 1976).

The activity of Complex IV was measured at 30 °C as the rate of cytochrome c oxidation, using a spectrophotometer (SpectraMax Plus 384, Molecular Devices) at 550 nm (Daley et al., 2005). A cytochrome c solution containing 10 mg/mL reduced cytochrome c (Sigma–Aldrich, St. Louis, MO, USA) and 50 mM Tris–HCl, pH 7.2, was prepared and an excess amount of sodium ascorbate (to saturation) was added. The excess sodium ascorbate was removed on a PD-10 column. The reaction mixture contained 25 μM cytochrome c in 50 mM Tris–HCl, pH 7.2. Reactions were initiated by adding the tissue homogenates (which contained 5.4–41 μg protein from WAT or 0.6–2.3 μg protein from BAT) to the reaction mixture. The final concentration of cytochrome c was 20 μM. The first order rate constant (k) was calculated from the natural logarithms of the absorbance after adding the tissue homogenates. These calculated values were then taken to be (k) and the activity was expressed in k/min/mg protein. Complex IV activities were also measured in the presence of 1 mM potassium ferricyanide as a blank (Daley et al., 2005).

2.9. RNA extraction and real-time reverse transcription-polymerase chain reaction (RT-PCR)

Total RNA was extracted from frozen WAT and BAT using RNAiso PLUS (Takara, Shiga, Japan), and was purified using the FastPure RNA kit (Takara), according to the manufacturer's protocol. To obtain cDNA, 1 μg RNA was subjected to reverse transcription by PrimeScript Reverse Transcriptase (Takara) with random hexamer primers (Takara). Real-time quantitative PCR was performed using the Applied Biosystems 7300 real-time PCR system (Life Technologies) with SYBR Premix ExTaqII (Takara), according to the manufacturer's instructions. Transcripts of PGC1α, Nuclear respiratory factor 1 (NRF1), Transcription factor A, mitochondrial (TFAM), Cytochrome c oxidase IV (COX4), UCP1, Fatty acid synthase (FAS) and TATA box binding protein (TBP) were amplified. TBP was used for normalization. Primer sequences are shown in Table 2.

2.10. Protein extraction and analysis of target protein levels by Western blot

WAT and BAT were lysed with lysis buffer (50 mM Tris–HCl, pH 6.8, 2% SDS and 5% glycerol), boiled for 5 min and sonicated. Protein concentrations of the soluble fraction were determined using the BCA protein Assay Kit, standardized by the addition of lysis buffer, 2-mercaptoethanol and bromophenol blue were added to the proteins to obtain final concentrations of 5% and 0.025%, respectively, and the samples boiled for 5 min. Equal amounts of proteins (5–20 μg) were subjected to SDS–PAGE and transferred to nitrocellulose membranes. Membranes were blocked with 2.5% skim milk and 0.25% BSA in Tris-buffered saline (50 mM Tris, pH 7.4, and 150 mM NaCl) containing 0.1% Tween 20 (TTBS) for 1 h at room temperature, and then probed with the appropriate primary antibodies overnight at 4 °C or for 2 h at room temperature. The primary antibodies for ATP-citrate lyase (Epitomics, Burlingame, CA, USA), ATP-citrate lyase pS455 (Epitomics) and β-actin (Sigma–Aldrich) were used. After washes with TTBS, membranes were incubated with the appropriate secondary antibody (horseradish peroxidase-conjugated $F(ab')_2$ fragment of goat anti-mouse IgG or anti-rabbit IgG; Jackson ImmunoResearch, West Grove, PA, USA), for 1 h at room temperature. After washing with TTBS, the membranes were incubated with ImmunoStar LD reagent (Wako). The specific proteins were visualized with LAS3000 (Fujifilm, Tokyo, Japan), and the data were analyzed using Multigauge software (Fujifilm).

2.11. Statistical analysis

All data derived from three to six rats in each group were expressed as means ± SEM and were examined using Student's t-test or Tukey's t-test. Differences with p values <0.05 were deemed statistically significant.

Table 2
Primer sequences for real-time RT-PCR.

	Forward	Reverse
PGC1α	5′-AGACGGATTGCCCTCATTTG-3′	5′-CAGGGTTTGTTCTGATCCTGTG-3′
NRF1	5′-TGATGAGGTAACTGCCCATCTG-3′	5′-TTGGAGGGTGAGATGCAGAG-3′
TFAM	5′-CGATTTTCTACAGAACAGCTACCC-3′	5′-GCTCTTTATACTTGCTCACAGCTTC-3′
COX4	5′-CATTTCTACTTCGGTGTGCCTTC-3′	5′-CACATCAGGCAAGGGGTAGTC-3′
UCP1	5′-CAGAGTTATAGCCACCACAGAAAGC-3′	5′-CAGGAGTGTGGTGCAAAACC-3′
FAS	5′-AGCAGGCACACACAATGGAC-3′	5′-GAAGAAGAAAGAGAGCCGGTTG-3′
TBP	5′-CAGTACAGCAATCAACATCTCAGC-3′	5′-CAAGTTTACAGCCAAGATTCACG-3′

PGC1α: peroxisome proliferator activated receptor gamma coactivator 1α; NRF1: nuclear respiratory factor 1; TFAM: mitochondrial transcription factor A; COX4: cytochrome c oxidase 4; UCP1: uncoupling protein 1; FAS: fatty acid synthase; TBP: TATA box binding protein.

3. Results

3.1. Histological analysis and triglyceride (TG) contents

CR markedly reduced body, WAT and BAT weights. CR also lowered the relative weight of WAT, but not of BAT, compared to the body weight (Table 1).

As shown in Fig. 1A and B, CR markedly reduced the size of lipid droplets. Because the unilocular lipid droplet occupies most of the cytoplasm of white adipocytes, the size of the lipid droplet is thought to represent the cell size. The median adipocyte size was 3203 μm^2 in the AL group and 2169 μm^2 in the CR group. The adipocyte size distribution was wider in AL rats compared with CR rats. The percentage of adipocytes that were larger than 8000 μm^2 was 6.6% in AL rats and less than 0.5% in CR rats. In contrast, the portion of adipocytes that were smaller than 2000 μm^2 was approximately 50% in CR rats and 33% in AL rats (Fig. 1A, B and E). Consistent with the histological data, CR significantly reduced TG content in the fasted state (Fig. 1G).

In BAT, brown adipocytes with multilocular lipid droplets of various sizes were observed. Moreover, many white adipocytes had infiltrated into the BAT. In BAT, it is difficult to distinguish the large lipid droplets in brown adipocytes from the white adipocytes that have infiltrated into BAT. Therefore, lipid droplet size is not thought to represent cell size. In contrast to WAT, large lipid droplets were predominantly observed in BAT from CR rats compared with AL rats. The median lipid droplet size was 123 μm^2 in AL rats and 191 μm^2 in CR rats. The proportion of lipid droplets larger than 300 μm^2 was more than 30% in CR rats and approximately 15% in the AL group (Fig. 1C, D and F). Consistent with the histological data, CR did not decrease TG content in the fasted state (Fig. 1H).

3.2. Proteome analysis

In WAT, proteome analysis revealed that CR increased the expression of five proteins and reduced the expression of two proteins (Fig. 2 and Table 3). The five proteins up-regulated by CR are involved in metabolic processes. ATP-citrate synthase (ACLY, Spot 1; Berwick et al., 2002; Ramakrishna and Benjamin, 1979), NADP-dependent malic enzyme (MAOX, Spot 2; Taroni and Di Donato, 1988) and long-chain specific acyl-CoA dehydrogenase, mitochondrial (ACADL, Spot 3; Ikeda et al., 1985) are lipid metabolism-related enzymes, and pyruvate dehydrogenase E1 component subunit beta, mitochondrial (ODPB, Spot 4; Huh et al., 1990) and pyruvate carboxylase, mitochondrial (PYC, Spot 5; Jitrapakdee et al., 2006) are glucose metabolism-related enzymes (Table 3). Moreover, three of these five proteins (ACADL, ODPB and PYC) are mitochondrial proteins. In contrast, expression of apolipoprotein A4 (APOA4, Spot 6), which is involved in cholesterol transport (Wang and Paigen, 2005), was attenuated by CR. CR also suppressed the expression of Heat shock protein beta 1 (HSPB1, Spot 7).

In BAT, proteome analysis revealed that CR reduced the expression of four proteins and increased the expression of five proteins (Fig. 3 and Table 4). All four proteins down-regulated by CR [Cytochrome c oxidase subunit 5B (COX5B, Spot 13), NADH dehydrogenase flavoprotein 1, mitochondrial (NAUV1, Spot 14), 2-oxoisovalerate dehydrogenase subunit beta (ODBB, Spot 15) and Succinyl-CoA ligase [ADP-forming] subunit beta, mitochondrial (SUCB1, Spot 16)] are mitochondrial metabolic enzymes. COX5B is one of the small polypeptide subunits composing Complex IV of the mitochondrial electron transport chain, a complex that also contains three large subunits (Capaldi, 1990). NAUV1 is a component of the flavoprotein-sulfur (FP) fragment of Complex I of the mitochondrial electron transport chain (Kerscher et al., 2008). ODBB, also known as branched-chain alpha-keto acid dehydrogenase E1 component alpha chain, catalyzes the reaction from 3-methyl-2-oxobutanoate to 2-methylpropanoyl-CoA, and participates in valine, leucine and isoleucine degradation (She et al., 2007). SUCB1 catalyzes the reaction from succinate to succinyl-CoA in the Krebs cycle (Lambeth et al., 2004). In contrast, Apolipoprotein A1 (APOA1, Spot 8), which is found predominantly in HDL-cholesterols and is involved in cholesterol transport (Wang and Paigen, 2005), was up-regulated by CR. The expression of Tubulin tyrosine ligase-like family, member 10 (TTLL10, Spot 11), which post-translationally modifies tubulin (Ikegami and Setou, 2009) and nucleosome assembly protein 1 (Jahnke et al., 2010), and of Glycerol kinase 5 (GLPK5, Spot 12) were also increased by CR. Interestingly, ACLY (Spot 9) and MAOX (Spot 10) were up-regulated by CR in BAT as well as in WAT. Glycerol kinase, which catalyzes the transfer of a phosphate from ATP to glycerol forming glycerol 3-phosphate, is a primary lipolytic enzyme (Watford, 2000). However, glycerol 3-phosphate is also a substrate for TG formation. Therefore, CR-associated up-regulation of GLPK5 as well as ACLY and MAOX might also activate lipogenesis in BAT (Fig. 3 and Table 4).

Thus, the proteome profile indicates that CR might activate mitochondrial function in WAT, while suppressing the mitochondrial electron transport chain and oxidative phosphorylation in BAT. However, it is likely that CR activates fatty acid biosynthesis similarly in both WAT and BAT.

3.3. Analysis of mitochondrial function

Based on the proteome profile, the relative content of mitochondrial DNA (mtDNA) was measured. The activities of the mitochondrial Krebs cycle enzyme, citrate synthase (CS), and the mitochondrial electron transport chain complex IV (cytochrome c oxidase) were also analyzed (Alp et al., 1976; Dumas et al., 2004; Wiegand and Remington, 1986). In WAT, CR increased the mtDNA content (Fig. 4A) and enhanced CS and complex IV activities in both the fed and fasted states (Fig. 4C). CR reduced the mtDNA content of BAT in the fed state, while fasting increased mtDNA content in CR rats (Fig. 4B). CR did not affect CS activity, but

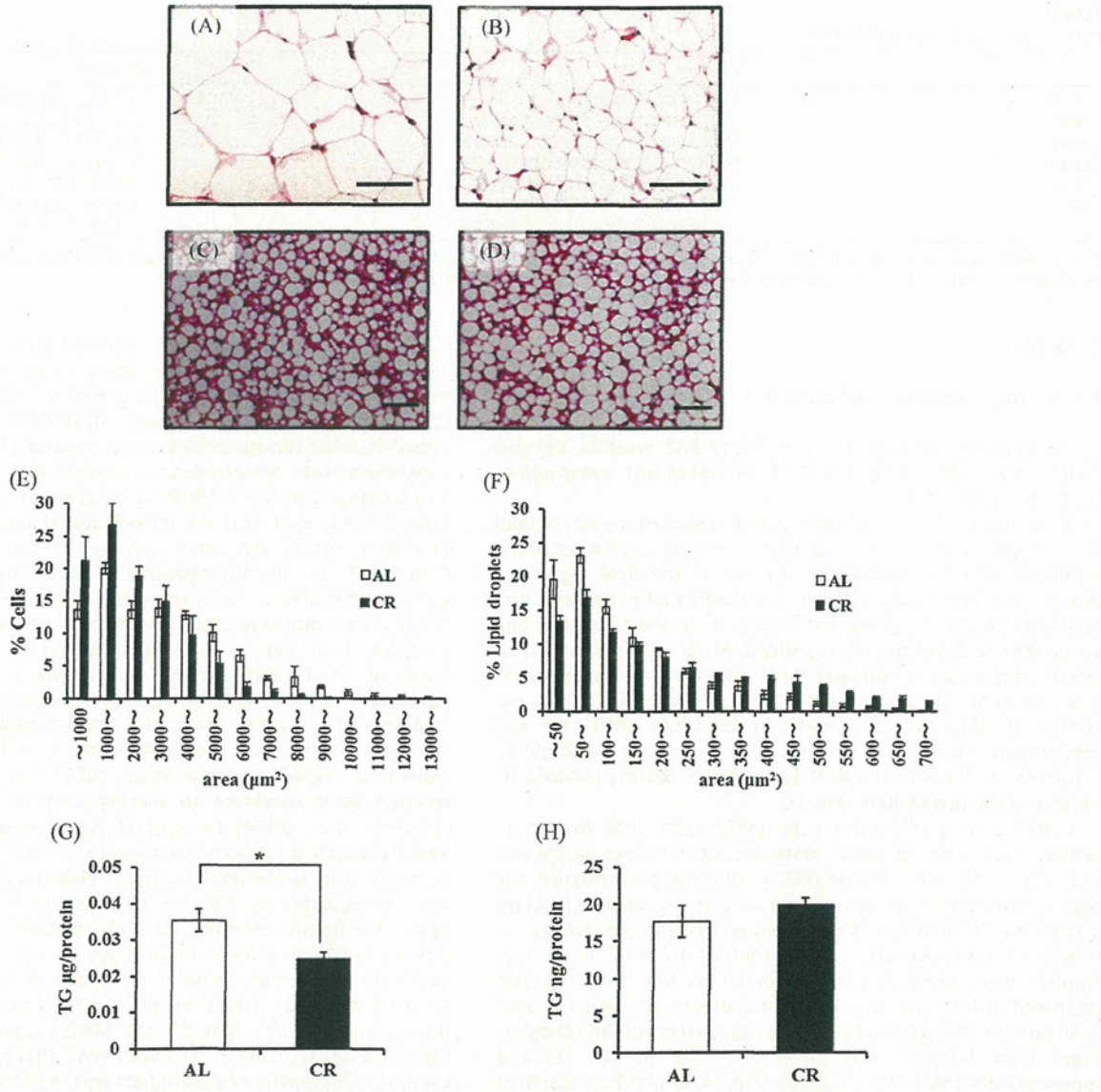

Fig. 1. CR-associated alteration of morphology and triglyceride content in WAT and BAT from AL and CR rats. Representative histological sections of WAT from AL (A) and CR (B) rats (magnification: 40×, scale bar: 100 μm), and of BAT from AL (C) and CR (D) rats (magnification: 200×, scale bar: 50 μm). Sections were stained with hematoxylin–eosin. Based on a quantitative morphometric method using "ImageJ 1.43u/Java1.6.0_22" software, the distribution of adipocyte size in WAT (E) and lipid droplet size in BAT (F) was measured. Triglyceride content of WAT (G) and BAT (H) was also measured. Values shown in all panels are means ± SEM of three to five animals in each group. $^{*}p < 0.05$ by Student's *t*-test.

fasting markedly suppressed it (Fig. 4D). However, Complex IV activity was only slightly reduced by CR (Fig. 4F).

The expression level of several mitochondrial biogenesis-related genes including PGC1α, NRF1, TFAM, COX4 and UCP1 was analyzed by real-time RT-PCR. PGC1α is a transcriptional co-activator that induces mitochondrial biogenesis by activating several transcription factors including NRF1 (Farmer, 2008; Liang and Ward, 2006; Puigserver and Spiegelman, 2003). NRF1 transcriptionally activates TFAM, which drives transcription and replication of the mitochondrial genome as well as transcription of a nuclear-encoded component of Complex IV of the mitochondrial electron transport chain, COX4 (Kang et al., 2007; Lenka et al., 1998; Liang and Ward, 2006; Puigserver and Spiegelman, 2003). The expression of UCP1, which is a BAT-specific protein that contributes to non-shivering thermogenesis, is also transcriptionally regulated *via* the activation of certain nuclear hormone receptors by PGC1α (Liang and Ward, 2006). In WAT, CR up-regulated the expression of PGC1α and COX4 in both fed and fasted states (Fig. 5A and D). CR did not affect the expression of NRF1, but it did increase TFAM levels in the fed state. TFAM expression was also up-regulated by fasting in the AL rats (Fig. 5B and C). In BAT, CR up-regulated the expression of PGC1α in the fed state (Fig. 5F). In contrast, CR down-regulated the expression of COX4, particularly in the fed state (Fig. 5I). CR also down-regulated the expression of both NRF1 and TFAM in the fed state, but not in the fasted state (Fig. 5G and H). Moreover, CR inhibited the expression of UCP1 in both fed and fast states (Fig. 5J).

3.4. Analysis of lipogenesis

As mentioned above, proteome analysis suggested that CR might activate lipogenesis in both WAT and BAT. To confirm these CR-associated changes, we further examined the expression of ACLY (Spot 1 in Fig. 2B and Spot 9 in Fig. 3B). In the 2-DE image of

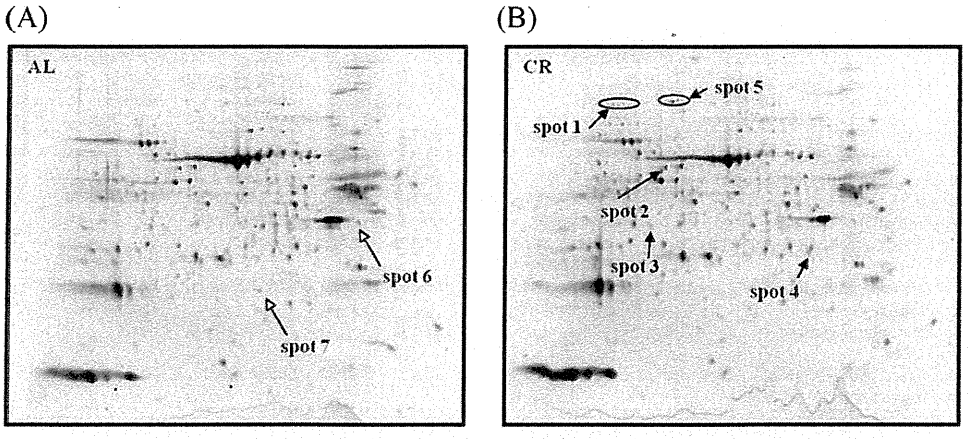

Fig. 2. CR-associated alteration of the protein expression profile of WAT as detected on representative gel images of 2-DE. Protein samples were extracted from WAT of AL-fed and CR-fed rats and separated in pH 3–10 IPG strips for the first dimension and 7.5% SDS–PAGE for the second dimension. Fluorescent gel images stained with SYPRO Ruby were obtained using a FluoroPhoreStar3000 and analyzed with Progenesis PG200 software. Open arrows indicate spots down-regulated by CR, and closed arrows indicate spots up-regulated by CR. 2-DE was performed in duplicate or triplicate for each sample with biological repeats of $n = 3$ for each group.

Table 3
Identified proteins, of which expression were changed by CR.

Spot number	Protein description	Function	MW (kDa)	Pi	NCBI accession number (gi)	Mascot score	Sequence coverage (%)	CR-fed/ AL-fed	CR-fast/ AL-fast
1	ATP-citrate synthase (ACLY)	Lipo genesis	121.47	6.96	113116	101	10	>>>	>>>
2	NADP-dependent malic enzyme (MAOX)	Lipo genesis	64.59	6.49	266504	–	–	5.08	3.23
3	Long-chain specific acyl-CoA dehydrogenase, mitochondrial (ACADL)	Mitochondrial beta-oxidation	48.24	7.63	113016	82	18	1.96	1.97
4	Pyruvate dehydrogenase E1 component subunit beta, mitochondrial (ODPB)	Glycolysis	39.30	6.20	122065728	124	35	>>>	>>>
5	Pyruvate carboxylase, mitochondrial (PYC)	Gluconeogenesis	130.44	6.34	146345499	130	16	3.85	3.17
6	Apolipoprotein A-4 (APOA4)	Cholesterol transport	44.43	5.12	114008	71	13	0.56	0.62
7	Heat shock protein beta-1 (HSPB1)	Stress response	22.94	6.12	1170367	123	30	0.63	0.32

>>>: Spots, which were not detected in AL-fed or AL-fast rats.

WAT and BAT, CR increased the intensity of Spot 1 and Spot 9, respectively. Moreover, CR increased the number of spots along the X-axis in both Spot 1 and Spot 9, suggesting that CR up-regulated ACLY protein levels and might have altered its post-translational modification in both WAT and BAT. Therefore, the phosphorylated form of ACLY (p-ACLY), which is the active form (Ramakrishna and Benjamin, 1979), and total ACLY (t-ACLY) levels were analyzed. In both WAT and BAT, CR increased p-ACLY and t-ACLY levels in both the fed and fasted states. Increased p-ACLY apparently results from an increased amount of t-ACLY (Fig. 6).

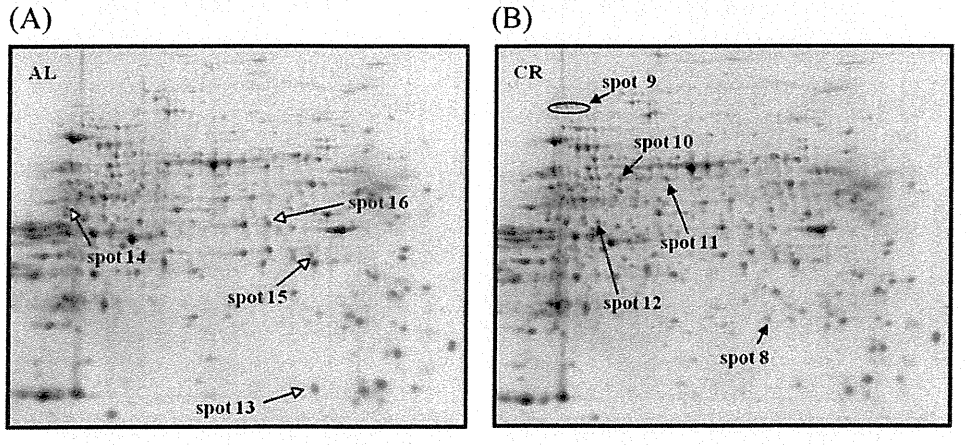

Fig. 3. CR-associated alteration of the protein expression profile of BAT as detected on representative gel images by two-dimensional gel electrophoresis. Protein samples were extracted from BAT of AL-fed and CR-fed rats and separated in pH 3–10 IPG strips for the first dimension and 7.5% SDS–PAGE for the second dimension. Fluorescent gel images stained with SYPRO Ruby were obtained using a FluoroPhoreStar3000 and analyzed with Progenesis PG200 software. Open arrows indicate spots down-regulated by CR, and closed arrows indicate spots up-regulated by CR. 2-DE was performed in duplicate or triplicate for each sample with biological repeats of $n = 3$ for each group.

Table 4
Identified proteins in BAT, of which expressions were changed by CR.

Spot number	Protein description	Function	MW (kDa)	Pi	NCBI accession number (gi)	Mascot score	Sequence coverage (%)	CR-fed/ AL-fed	CR-fast/ AL-fast
8	ApolipoproteinA-1 (APOA1)	Cholesterol transport	30.10	5.52	146345369	80	27	3.77	1.39
9	ATP-citrate synthase (ACLY)	Lipogenesis	121.47	6.96	113116	–	–	2.53	2.27
10	NADP-dependent malic enzyme (MAOX)	Lipogenesis	64.59	6.49	266504	–	–	2.17	3.07
11	Protein polyglycylase TTLL10 (TTL10)	Composition of nicrotuble	78.00	9.55	172045959	52	8	1.93	1.42
12	Putative glycerol kinase 5 (GLPK5)	Lipogenesis	60.34	6.84	172046763	75	14	2.36	1.69
13	Cytochrome c oxidase subunit 5B (COX5B)	Electron transport and oxidative phosphorylation	14.19	7.68	1352167	60	31	0.46	0.64
14	NADH dehydrogenase flavoprotein 1, nitochondrial (NDUV1)	Electron transport and oxidative phosphorylation	51.85	8.51	47117274	82	15	0.60	0.49
15	2-Oxoisovalerate dehydrogenase subunit beta (ODBB)	Branched chain arrrino acid metabolism	43.54	6.41	161784344	54	17	0.57	0.60
16	Succinyl-CoA ligase [ADP-forming] subunit beta, mitochondrial (SUCB1)	Krebs cycle	50.42	6.57	52788305	64	14	0.65	0.49

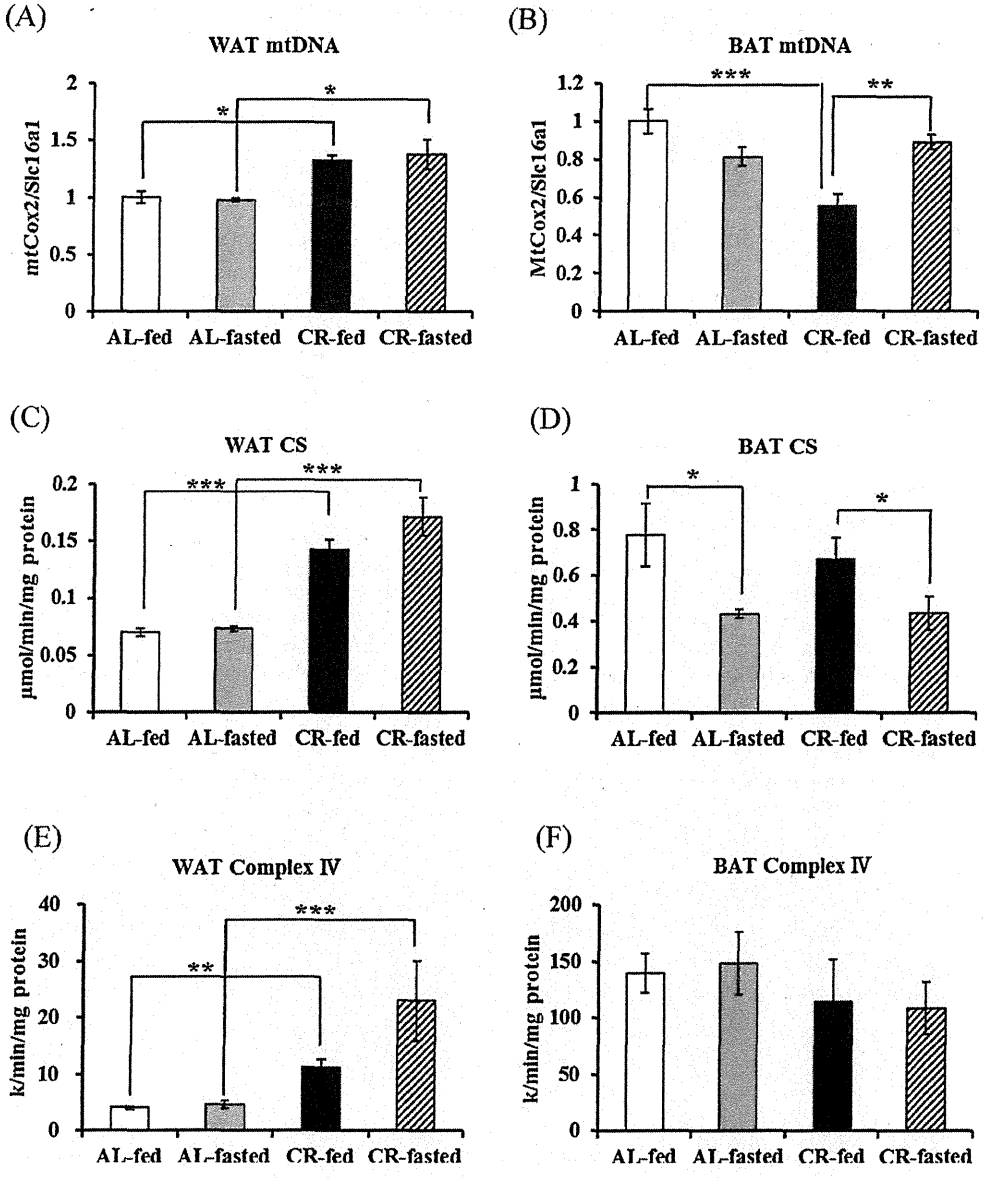

Fig. 4. Effects of CR on mitochondrial DNA content and enzyme activity in WAT and BAT. The ratio of mitochondrial (COX2) *vs.* nuclear (SLC16A1) DNA was obtained by real-time PCR in WAT (A) and BAT (B). Ratios are expressed as the fold change relative to the mean value of AL-fed rats. Citrate synthase activity in WAT (C) and BAT (D) was measured spectrophotometrically at 412 nm. Activity of electron transport chain complex IV and cytochrome c oxidase was measured spectrophotometrically at 550 nm in WAT (E) and BAT (F). Values shown in all panels are means ± SEM of three to five animals in each group. $^{*}p < 0.05$, $^{**}p < 0.01$. $^{***}p < 0.001$ by Tukey's *t*-test.

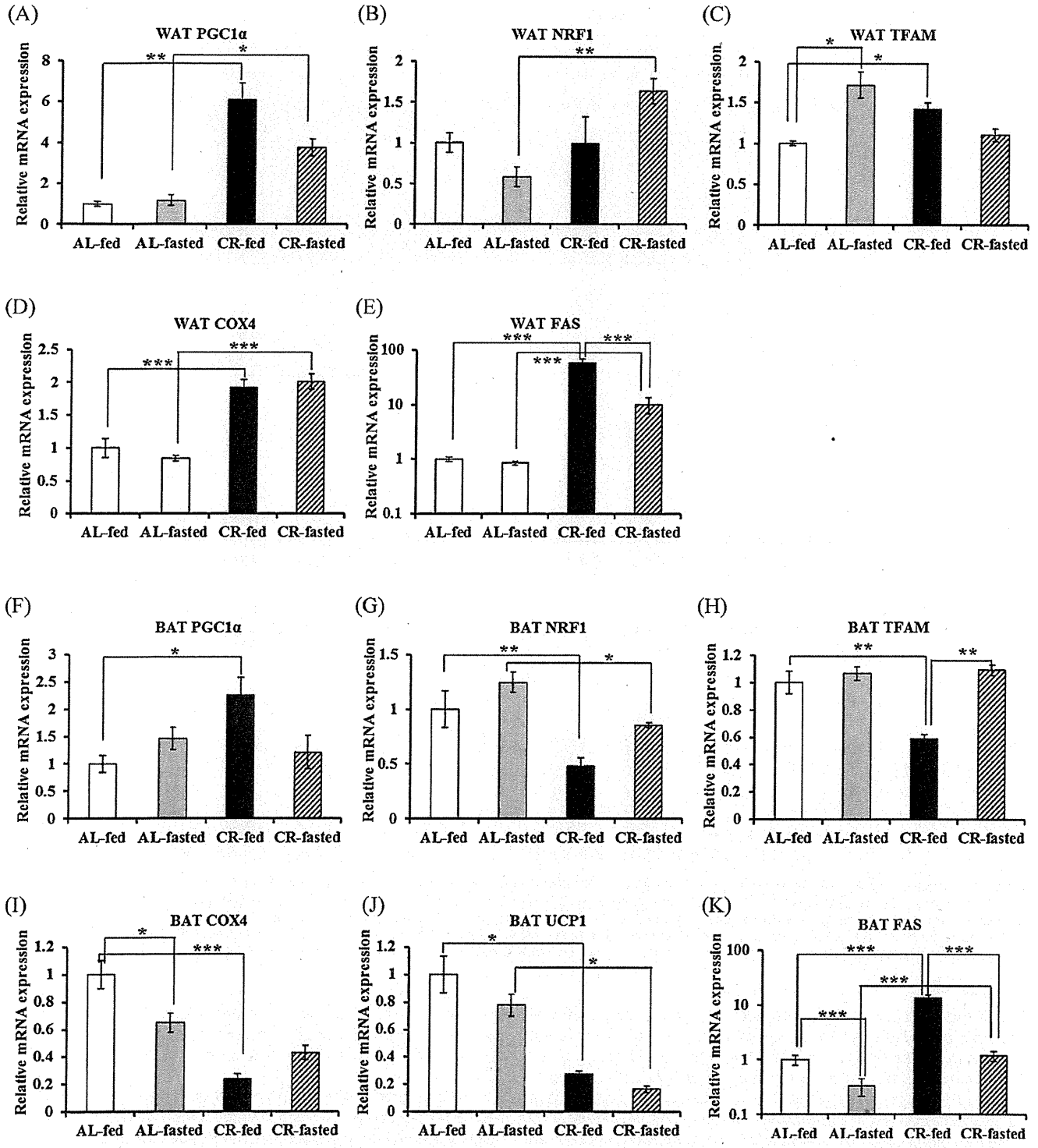

Fig. 5. Effects of CR on the expression of genes involved in mitochondrial biogenesis and fatty acid biosynthesis in WAT (A–E) and BAT (F–K). The mRNA levels of PGC1α (A and F), NRF1 (B and G), TFAM (C and H), COX4 (D and I), UCP1 (J) and FAS (E and K) were determined by real-time RT-PCR. The average intensity of each product was relative to the control gene TBP. Values shown in all panels are means ± SEM of three to five animals in each group, and are expressed as the fold change relative to the mean value of AL-fed rats. $^{*}p < 0.05$, $^{**}p < 0.01$. $^{***}p < 0.001$ by Tukey's *t*-test.

Fatty acid synthase (FAS) plays a central role in *de novo* lipogenesis (Griffin and Sul, 2004). In WAT and BAT, the mRNA levels of FAS were up-regulated by CR in both fed and fast states (Fig. 5E and K). Therefore, it is likely that CR activates fatty acid biosynthesis in both WAT and BAT. In AL rats, however, fasting suppressed FAS expression in BAT but not in WAT.

4. Discussion

4.1. WAT response to CR

In WAT of CR rats, the adipocytes had a relatively small and uniform size. The morphological change induced by CR was

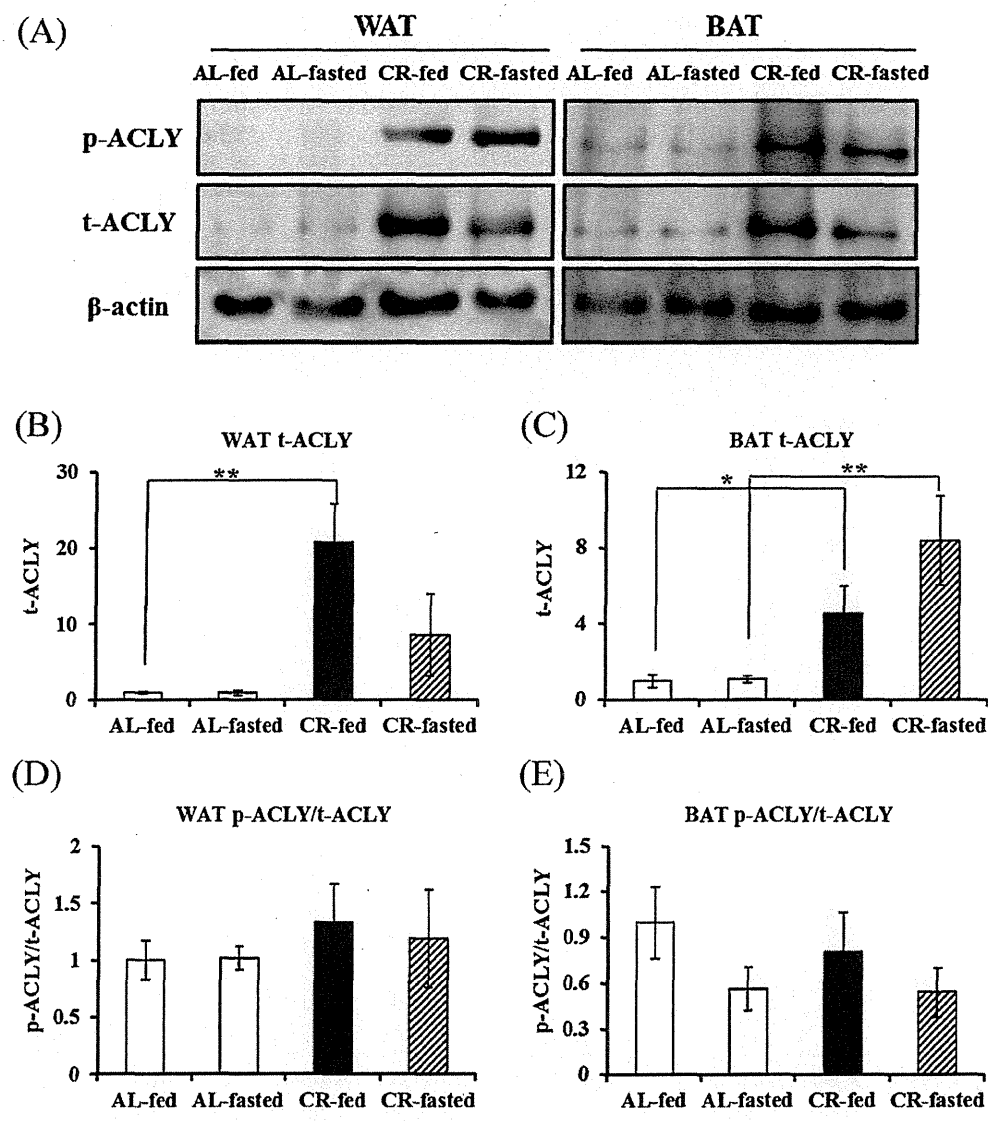

Fig. 6. CR-associated alteration of phosphorylation levels of ACLY in WAT and BAT. Protein samples were extracted from WAT and BAT of AL-fed, AL-fasted, CR-fed and CR-fasted rats. Western blot analysis of total ACLY (t-ACLY) and phosphorylated form of ACLY (p-ACLY) was performed using the chemiluminescence method. The specific proteins were visualized using an LAS3000 image analyzer. Both β-actin and the intensity of CBB stain were used as a normalization control. Western blot analysis was performed in duplicate or triplicate from each sample with biological repeats of $n = 5$ for each group. A representative gel image of the Western blot is shown (A). Densitometry data of t-ACLY (B and C) and p-ACLY/t-ACLY (D and E) were measured, and are shown for WAT (B and D) and BAT (C and E).

associated with reduced TG content. In contrast, adipocytes of various sizes, including large hypertrophic adipocytes, were found in AL rats. These findings confirm previous data (Higami et al., 2004; Zhu et al., 2007). In general, excessive energy associated with excessive food intake is accumulated in adipocytes in the form of TG. The excessive TG accumulation is initially compensated for by increased adipocyte size. Further TG accumulation induces an increased number of adipocytes *via* proliferation of preadipocytes (Sakai et al., 2007). Therefore, it is likely that in AL rats the excessive energy supply was compensated for by both increased size and increased number of adipocytes in WAT. In CR rats, such compensation is not required due to the lower energy supply. It is well known that small adipocytes secrete more adiponectin and less pro-inflammatory cytokines, such as TNFα and leptin (Higami et al., 2005; Zhu et al., 2007). In addition, small adipocytes are generally more sensitive to insulin and act as powerful buffers absorbing lipids in the postprandial period. Hence, it appears that the small-sized white adipocytes observed in CR rats are more sensitive to insulin, secrete more adiponectin and less pro-inflammatory adipokines, and have a more powerful buffering activity for lipids (Frayn, 2002; Higami et al., 2005; Zhu et al., 2007).

All five proteins shown to be up-regulated in WAT by CR are metabolic enzymes involved in lipid metabolism (ACLY, MAOX and ACADL) and glucose metabolism (ODPB and PYC). Previously, it had been demonstrated by DNA microarray analysis that most genes up-regulated by CR are involved in metabolic processes (Higami et al., 2004, 2006b). Using proteome analysis in WAT, we showed that CR up-regulates three mitochondrial enzymes: ACADL, ODPB and PYC. ACADL is involved in β-oxidation of long-chain fatty acids (Ikeda et al., 1985). ODPB is an E1 component beta subunit of the pyruvate dehydrogenase (PDH) complex (Huh et al., 1990). The mitochondrial PDH complex catalyzes the conversion of pyruvate to acetyl-CoA and CO_2, linking glycolysis to the Krebs cycle and fatty acid biosynthesis (Sugden and Holness, 2003). PYC catalyzes the carboxylation of pyruvate to oxaloacetate (Jitrapakdee et al.,

2006). Thus, our finding supports previous reports showing that CR promotes mitochondrial biogenesis in WAT (Anderson and Prolla, 2009; Nisoli et al., 2005). To confirm the CR-associated mitochondrial activation, we analyzed mitochondrial function by measuring mtDNA contents, mRNA levels of PGC1α, NRF1, TFAM and COX4, and the activities of CS and Complex IV of the mitochondrial respiratory transport chain. We found that in both the fed and fasted states, CR increased mtDNA content, CS and Complex IV activities, and mRNA expression levels of PGC1α and COX4. Moreover, CR enhanced the expression of NRF1 in the fasted state and of TFAM in the fed state. Thus, CR activates various mitochondrial metabolic processes (Anderson and Prolla, 2009; Higami et al., 2004; Nisoli et al., 2005). The activity scale of CS was higher in BAT compared with WAT (Fig. 4C and D); however, when examining the activity of Complex IV this difference was markedly larger (Fig. 4E and F, note the *Y*-axis scales). Therefore, the Krebs cycle may have a more dominant function than the respiratory transport chain in WAT compared with BAT.

Proteome analysis also revealed that the expression of both ACLY and MAOX, which are cytoplasmic enzymes involved in lipid metabolism, was increased by CR. ACLY catalyzes the conversion of citrate and CoA to acetyl-CoA and oxaloacetate (Ramakrishna and Benjamin, 1979). Therefore, it is the primary enzyme responsible for the synthesis of cytosolic acetyl-CoA. The product, acetyl-CoA, serves as a substrate for important biosynthetic pathways, including lipogenesis. MAOX catalyzes oxidative decarboxylation of malate to pyruvate (Taroni and Di Donato, 1988). Importantly, MAOX generates NADPH, which is a critical fatty acid biosynthesis substrate (Taroni and Di Donato, 1988). FAS plays a central role in *de novo* fatty acid biosynthesis by converting acetyl-CoA and malonyl-CoA into the final end product, palmitate, which can subsequently be esterified into triacylglycerols and then stored in adipose tissue (Griffin and Sul, 2004). The mRNA level of FAS was up-regulated by CR in WAT. Thus, our data suggest that CR activates fatty acid biosynthesis in both the fed and fasted states. Recent proteome analysis also found that CR enhanced the expression of MAOX and FASN in WAT of rats at 24 months of age (Valle et al., 2010). This suggests that maintaining enhanced *de novo* fatty acid biosynthesis throughout life may be an important beneficial action of CR.

Proteome analysis also found that CR suppressed the expression of HSPB1. It has been reported that HSPB1, a molecular chaperone that protects partially mis-folded proteins (particularly during oxidative stress), is up-regulated by a high-fat diet (Balwierz et al., 2009; Dosh et al., 2010). Our finding is consistent with the interpretation that the expression of this protein is reduced because CR attenuates oxidative stress and thus the requirement for this chaperone may be decreased (Wang and Paigen, 2005).

4.2. BAT response to CR

In contrast to WAT, CR enlarged the lipid droplets in BAT. Because white adipocytes tend to infiltrate into BAT with aging, the lipid droplets observed in BAT were probably derived from both unilocular lipid droplets of infiltrating small white adipocytes and multilocular lipid droplets in brown adipocytes. In fact, CR showed some evidence of up-regulation of the mRNA level of leptin (a white adipocyte marker) in BAT in both the fed and fasted states, although this was not statistically significant (unpublished data). Together, these results suggest that CR could promote the infiltration of white adipocytes into BAT as well as the accumulation of TG in multilocular lipid droplets in brown adipocytes.

Proteome analysis of BAT demonstrated reduced expression of four mitochondrial enzymes (COX5B, NAUV1, ODBB and SUCB1) in response to CR; two out of these proteins (COX5B, NAUV1) are involved in the electron transport chain. Consistent with the observed proteome profiles, CR significantly suppressed mRNA levels of COX4 in the fed state. Moreover, CR markedly reduced mtDNA content and mRNA levels of NRF1 and TFAM in the fed state, and mRNA levels of UCP1 in both fed and fasted states. In contrast, the level of PGC1α mRNA was up-regulated by CR in the fed state. Fasting did not change mtDNA content, or the expression levels of NRF1 and TFAM, in AL rats, but it increased these parameters in CR rats. In BAT, mtDNA content roughly correlated with the expression levels of NRF1 and TFAM, but inversely correlated with the expression of PGC1α. It is well known that PGC1α is a master regulator of mitochondrial biogenesis and UCP1 transcription (Puigserver and Spiegelman, 2003). However, CR- or fasting-induced expression of PGC1α did not correlate with the expression of UCP1. Further examination is required to elucidate this discrepancy.

In BAT, CR did not markedly affect the activities of either CS or Complex IV. Moreover, CR suppressed the expression of mitochondria-related genes including NRF1, TFAM COX4 and UCP1, suggesting that, in contrast to WAT, CR does not activate mitochondrial function. However, as was observed in WAT, levels of the cytoplasmic enzymes ACLY and MAOX (Berwick et al., 2002; Ramakrishna and Benjamin, 1979; Taroni and Di Donato, 1988), and the mRNA level of FAS were up-regulated by CR. Furthermore, we found that CR induced ACLY phosphorylation, suggesting that CR promotes fatty acid biosynthesis in BAT as well as in WAT. CS catalyzes the reaction from acetyl-CoA and oxaloacetate to citrate, which is the first step of the Krebs cycle (Alp et al., 1976; Wiegand and Remington, 1986). Citrate is used as a substrate for the Krebs cycle in mitochondria, as well as a substrate for ACLY when exported from the mitochondria to the cytoplasm. Therefore, it may be important to maintain CS activity to promote lipogenesis even under the CR condition. In contrast, fasting reduced CS activity and the mRNA level of FAS, suggesting that fasting might suppress lipogenesis by reducing the citrate supply from mitochondria.

As mentioned above, our data suggest that CR activates various mitochondrial functions, including the Krebs cycle and the electron transport chain, in WAT. It also accelerates fatty acid biosynthesis. We consider, therefore, that CR animals use glucose predominantly in glucose-dependent organs such as the central nervous system after feeding. To use energy effectively under the condition of energy shortage, residual glucose could be converted to more energy-dense fatty acids in WAT. Then, the newly generated fatty acids might be stored in the form of TG in WAT and BAT, and/or be supplied to and used in non-glucose-dependent organs. In other words, it is likely that WAT in CR rats functions as an energy transducer from glucose to more energy-dense lipids and not as an energy storage system (Fig. 7A). In BAT, CR suppresses mitochondrial function, but activates fatty acid biosynthesis. It is likely that in CR rats BAT functions as an energy reservoir system in the form of TG (Fig. 7B). Thus, CR-associated functional alteration of mitochondria significantly differs between WAT and BAT, while it is likely that CR activates fatty acid biosynthesis and the metabolic process involving pyruvate, citrate, oxaloacetate and malate in both WAT and BAT. This metabolic process is known as pyruvate/malate cycling (Salway, 1999) or pyruvate/citrate cycling (Guay et al., 2007; Jensen et al., 2008). NADPH, which is generated by the pentose phosphate pathway and the chemical reaction catalyzed by malic enzyme (MAOX) in pyruvate/malate cycling, is a pivotal coenzyme for fatty acid biosynthesis. When energy supply is not sufficient, such as in CR animals, glucose is converted to pyruvate in the glycolytic pathway and does not mobilize to the pentose phosphate pathway. Therefore, we believe that in CR animals NADPH, which is vital for fatty acid biosynthesis, is predominantly generated by pyruvate/malate cycling. ACLY and MAOX, which are up-regulated by CR in both WAT and BAT, are involved in this cycle. Recently, it has been reported that certain enzymes including ODPB and malate dehydrogenase, which are

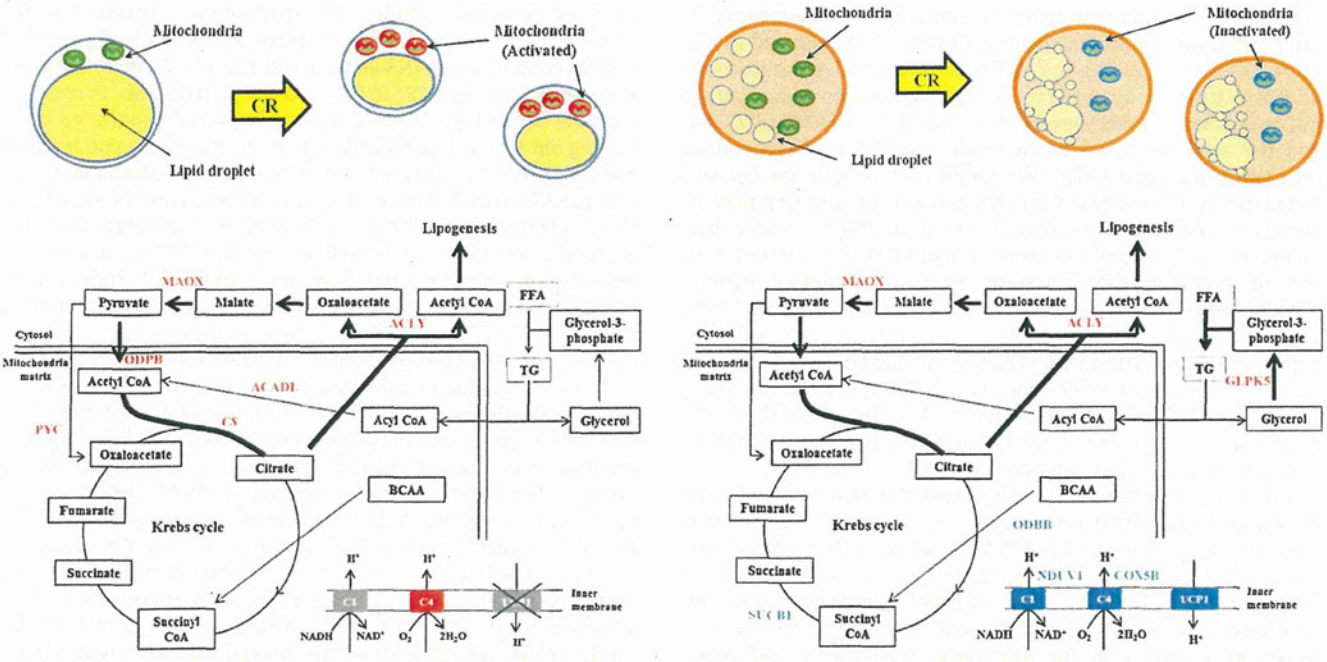

Fig. 7. *Schematic diagram of the differential responses of WAT and BAT to CR based on the present study. In WAT, CR activates various mitochondrial functions including the* Krebs cycle and the electron transport chain. It also accelerates fatty acid biosynthesis. It is likely that in CR rats WAT functions as an energy transducer from glucose to more energy-dense lipids and not as an energy storage system (A). In BAT, CR does not activate mitochondrial functions, but activates fatty acid biosynthesis. It is likely that in CR rats BAT functions as an energy reservoir system in the form of TG (B). CR-associated functional alterations of mitochondria significantly differ between WAT and BAT. However, it is likely that CR activates fatty acid biosynthesis and pyruvate/citrate cycling in both WAT and BAT. Expression of genes or proteins and enzymatic activities that were up-regulated by CR are indicated by red letters, and those down-regulated by CR are indicated by blue letters. ACADL: long-chain specific acyl-CoA dehydrogenase, mitochondrial; ACLY: ATP-citrate synthase; COX4: cytochrome c oxidase 4; COX5B: cytochrome c oxidase subunit 5B; CS: citrate synthase; FFA: free fatty acid; GLPK5: glycerol kinase 5; MAOX: NADP-dependent malic enzyme; NDUV1: NADH dehydrogenase flavoprotein 1, mitochondrial; ODBB: 2-oxoisovalerate subunit beta; ODPB: pyruvate dehydrogenase E1 component subunit beta, mitochondrial; PYC: pyruvate carboxylase, mitochondrial; SUCB1: succinyl-CoA ligase [ADP-forming] subunit beta, mitochondrial; TG: triglyceride; UCP1: uncoupling protein 1.

involved in pyruvate/malate cycling, are important regulators of lifespan in yeast (Easlon et al., 2007, 2008). Therefore, pyruvate/malate cycling may be a novel key regulator of the anti-aging and pro-longevity effects of CR.

Based on our data, we conclude that CR activates *de novo* fatty acid biosynthesis in both WAT and BAT. In contrast, CR enhances mitochondrial function in WAT but does not in BAT. The remodeling of both WAT and BAT, which is characterized by effective energy utilization, may promote beneficial actions associated with CR.

Acknowledgements

We thank all members of the Molecular Pathology and Metabolic Disease and Animal Center of Faculty of Pharmaceutical Sciences, Tokyo University of Science, for their cooperation. We also thank Professor Isao Shimokawa, Yutaka Araki and Yuko Moriyama in the Department of Investigative Pathology, Nagasaki University Graduate School of Biomedical Sciences, for their invaluable technical assistance. This work was partially supported by a Grant-in-Aid for Scientific Research (C) from the Japan Society for the Promotion of Science (19590396) and a Grant-in-Aid for the Third-term Comprehensive 10-year Strategy for Cancer Control from the Ministry of Health, Labor and Welfare, Japan.

References

Alp, P.R., Newsholme, E.A., Zammit, V.A., 1976. Activities of citrate synthase and NAD+-linked and NADP+-linked isocitrate dehydrogenase in muscle from vertebrates and invertebrates. Biochem. J. 154, 689–700.

Anderson, R., Prolla, T., 2009. PGC-1alpha in aging and anti-aging interventions. Biochim. Biophys. Acta 1790, 1059–1066.

Argmann, C., Dobrin, R., Heikkinen, S., Auburtin, A., Pouilly, L., Cock, T.A., Koutnikova, H., Zhu, J., Schadt, E.E., Auwerx, J., 2009. Ppargamma2 is a key driver of longevity in the mouse. PLoS Genet. 5, e1000752.

Balwierz, A., Polus, A., Razny, U., Wator, L., Dyduch, G., Tomaszewska, R., Scherneck, S., Joost, H., Dembinska-Kiec, A., 2009. Angiogenesis in the New Zealand obese mouse model fed with high fat diet. Lipids Health Dis. 8, 13.

Barzilai, N., Banerjee, S., Hawkins, M., Chen, W., Rossetti, L., 1998. Caloric restriction reverses hepatic insulin resistance in aging rats by decreasing visceral fat. J. Clin. Invest. 101, 1353–1361.

Berwick, D.C., Hers, I., Heesom, K.J., Moule, S.K., Tavare, J.M., 2002. The identification of ATP-citrate lyase as a protein kinase B (AKT) substrate in primary adipocytes. J. Biol. Chem. 277, 33895–33900.

Blüher, M., Michael, M.D., Peroni, O.D., Ueki, K., Carter, N., Kahn, B.B., Kahn, C.R., 2002. Adipose tissue selective insulin receptor knockout protects against obesity and obesity-related glucose intolerance. Dev. Cell 3, 25–38.

Blüher, M., Kahn, B.B., Kahn, C.R., 2003. Extended longevity in mice lacking the insulin receptor in adipose tissue. Science 299, 572–574.

Capaldi, R.A., 1990. Structure and assembly of cytochrome c oxidase. Arch. Biochem. Biophys. 280, 252–262.

Chiu, C.H., Lin, W.D., Huang, S.Y., Lee, Y.H., 2004. Effect of a C/EBP gene replacement on mitochondrial biogenesis in fat cells. Genes Dev. 18, 1970–1975.

Colman, R.J., Anderson, R.M., Johnson, S.C., Kastman, E.K., Kosmatka, K.J., Beasley, T.M., Allison, D.B., Cruzen, C., Simmons, H.A., Kemnitz, J.W., Weindruch, R., 2009. Caloric restriction delays disease onset and mortality in rhesus monkeys. Science 325, 201–204.

Daley, E., Wilkie, D., Loesch, A., Hargreaves, I.P., Kendall, D.A., Pilkington, G.J., Bates, T.E., 2005. Chlorimipramine: a novel anticancer agent with a mitochondrial target. Biochem. Biophys. Res. Commun. 328, 623–632.

DeClercq, V., Taylor, C., Zahradka, P., 2008. Adipose tissue: the link between obesity and cardiovascular disease. Cardiovasc. Hematol. Disord. Drug Targets 8, 228–237.

Dosh, B.M., Hightower, L.E., Lee, J., 2010. HSPB1, actin filament dynamics, and aging cells. Ann. N.Y. Acad. Sci. 1197, 76–84.

Dumas, J.F., Roussel, D., Simard, G., Douay, O., Foussard, F., Malthiery, Y., Ritz, P., 2004. Food restriction affects energy metabolism in rat liver mitochondria. Biochim. Biophys. Acta 1670, 126–131.

Easlon, E., Tsang, F., Dilova, I., Wang, C., Lu, S.P., Skinner, C., Lin, S.J., 2007. The dihydrolipoamide acetyltransferase is a novel metabolic longevity factor and is required for calorie restriction-mediated life span extension. J. Biol. Chem. 282, 6161–6171.